

UNCLASSIFIED

AD NUMBER
AD138244
NEW LIMITATION CHANGE
TO Approved for public release, distribution unlimited
FROM No Foreign
AUTHORITY
USNASC ltr. 20 Jan 83

THIS PAGE IS UNCLASSIFIED

UNCLASSIFIED

A138244

Armed Services Technical Information Agency

Reproduced by

DOCUMENT SERVICE CENTER

KNOTS BUILDING, DAYTON, 2, OHIO

FOR
REPRODUCTION
CONTROL ONLY

1 OF 2

THIS DRAWING IS
NOT TO BE USED FOR
GOVERNMENT
PURPOSES UNLESS
SPECIFICALLY
APPROVED BY THE
GOVERNMENT
SAID DRAWING
HAS NO
IMPLICATION
PERSON OR
USE OR SALE

GOVERNMENT OR OTHER DRAWINGS, SPECIFICATIONS OR OTHER DATA
BY PURPOSE OTHER THAN IN CONNECTION WITH A DEFINITELY RELATED
REQUIREMENT OPERATION, THE U. S. GOVERNMENT THEREBY INCURS
TY, NOR ANY OBLIGATION WHATSOEVER; AND THE FACT THAT THE
AY HAVE FORMULATED, FURNISHED, OR IN ANY WAY SUPPLIED THE
SPECIFICATIONS, OR OTHER DATA IS NOT TO BE REGARDED BY
OTHERWISE AS IN ANY MANNER LICENSING THE HOLDER OR ANY OTHER
ORATION, OR CONVERTING ANY RIGHTS OR PERMISSION TO MANUFACTURE,
7 PATENTED INVENTION THAT MAY IN ANY WAY BE RELATED THERETO.

UNCLASSIFIED

AD NO. 7
ACTIA

RADIATION FROM
LABORATORY SCALE
JET COMBUSTOR FLAMES

OCTOBER, 1956

PHILLIPS PETROLEUM COMPANY
RESEARCH AND DEVELOPMENT DEPARTMENT
BARTLESVILLE, OKLAHOMA



PHILLIPS PETROLEUM COMPANY

RESEARCH DIVISION

BARTLESVILLE, OKLAHOMA

SPECIAL REPORT

FOR

NAVY CONTRACT N0as 52-132-c

RADIATION FROM

LABORATORY SCALE JET

COMBUSTOR FLAMES

E. C. Miller

A. E. Blake

R. M. Schirmer

G. D. Kittredge

E. H. Fromm

RADIATION FROM LABORATORY SCALE JET COMBUSTOR FLAMES

44

by

E. C. Miller, A. E. Blake, R. M. Schirmer, G. D. Kittredge, and E. H. Fromm

S U M M A R Y

Characteristics of the energy radiated from aircraft gas turbine type combustion processes were investigated by Phillips Petroleum Company for the Navy Bureau of Aeronautics under Contract NOas 52-132-c. The study was conducted in Phillips' Jet Fuel Test Facility using a 2-inch combustor. Two paraffinic test fuels, normal heptane and isooctane, and two aromatic test fuels, benzene and toluene, were selected to obtain a wide range in hydrocarbon structure. They were metered to the combustor at an overall fuel-air ratio of 0.01. Three different test conditions were selected to be representative of ramjet, current turbojet, and future turbojet powerplants. Respective operating pressures were 40, 150, and 450 in. Hg abs. Infrared flame emission and absorption spectra, from 1 to 15 microns in wavelength, were obtained at five different locations around the combustor. This was also done without combustion, and without fuel; to obtain fuel, and air, absorption spectra. Supplementary measurements of four other combustion cleanliness parameters were also obtained for correlation purposes; i.e., combustor metal temperature, combustor fuel loss rate, combustor deposit formation rate, and exhaust gas smoke density.

Non-luminous flames were characterized by discontinuous radiation of molecular origin. Luminous flames were characterized by a predominance of continuous, black body type, radiation. At intermediate values of luminosity the discontinuous molecular radiation was evident, superimposed on the continuous radiation. The average transverse emissivity of the infrared spectral region for non-luminous flames was approximately 0.03; but it increased, with increasing flame luminosity, to nearly one.

The transverse emissivity of the flames increased with increasing combustor pressure, but the rate varied with fuel type. In general, flame emissivities of the aromatic fuels, benzene and toluene, were higher than those of the paraffinic fuels, normal heptane and isooctane. However, absorption by the smoke in the exhaust column decreased the longitudinal emissivity of the two aromatic fuels with increasing pressure at higher pressures. This corroborates indications of even more extensive reversals in emissivity, previously observed at higher smoke densities than obtained during this study.

----- (continued) -----

OCT 26 1956

This copy of this report has been released for private information only, and with the understanding that any other use of the subject matter, in whole or in part, by reference or otherwise, shall be only with the knowledge of Phillips Petroleum Company, and with the approval of that company first obtained; and with the further understanding that this report is prepared and submitted for informative purposes only and that any suggestions and recommendations contained herein shall not be understood or construed as, in any sense, guarantees or warranties of any method, product or device.

S U M M A R Y (continued)

Energy transferred by radiation to combustor parts such as the flame tube, was an appreciable portion of the total energy released in luminous flames. The radiative power varied from less than one per cent to greater than ten per cent of the total energy released, depending upon experimental conditions.

The variations in combustor metal temperature, which accompanied changes in experimental conditions, followed total radiant energy trends. While the temperature of the flames remained essentially constant at 2800 F over a broad range of experimental conditions, indicating a constant extent of combustion; the combustor flame tube metal temperature varied over a 500 F range, in direct relation to the emissivity of the flame. In addition, the rate of metal loss, or burn off, from the combustor flame tube, which should be some index of combustor durability, also correlated with flame emissivity and the accompanying flame tube metal temperature.

The smoke forming tendency of the combustion process is important because it governs both flame radiative characteristics and transmission properties. In agreement with flame emissivity trends, the exhaust gas smoke density increased with increasing combustor pressure, and was highest for the two aromatic fuels. Flame tube deposit formation rates peaked at the intermediate pressure, 150 in. Hg abs, and were very low at the highest operating pressure, 450 in. Hg abs, with all four test fuels. As concluded during previous studies, this is taken as an indication of the ignition, and burn off, of deposits from the hotter flame tube metal walls, rather than a reduction in the rate of pyrolytic carbon formation at the higher combustor operating pressure.

Radiative energy transfer from the flame zone to the hydrocarbon fuel was relatively inefficient due to the non-coincidence of the absorption spectra of the atomized fuel and the emission spectra of the flame. The raw fuel absorbed over a spectral region containing only about ten per cent of the available energy from luminous flames, and less from non-luminous flames. Despite this inefficiency, the hydrogen was probably stripped from the carbon chains almost immediately, since little hydrocarbon as such was present in the flame zone of the combustor.

Total radiation pyrometers must include the 4 to 5 micron spectral region to give reliable indications of the total infrared radiation emitted by jet combustor type flames. For low luminosity flames sapphire optics will give substantially more reliable results than quartz optics. If pyrometric observations are made through long columns of exhaust gases, it may be necessary to take into account the absorption due to the combustion products and smoke.

The emissivity of the carbon dioxide 4 to 5 micron band was nearly one over a large range of operating conditions and fuel type. Indications are that the intensity of radiation in this spectral region should serve as a good index of the flame temperature, since it would be essentially independent of flame luminosity and atmospheric absorption, if a narrow band-pass pyrometer were used.

TABLE OF CONTENTS

	<u>Page</u>
SUMMARY	11
I. INTRODUCTION	1
II. TEST PROGRAM	2
III. EXPERIMENTAL SET-UP	6
A. Spectrophotometer Details	8
B. Combustor Details	14
IV. INFRARED SPECTRAL MEASUREMENTS	16
A. Emission Spectra	16
B. Absorption Spectra	27
V. DISCUSSION	32
A. Infrared Spectra	32
B. Black-Body Considerations	35
C. Flame Temperature	38
D. Total Radiation Measurement	40
E. Combustion Process	48
VI. SUPPLEMENTARY MEASUREMENTS OF COMBUSTION CLEANLINESS	48
A. Combustor Metal Temperature	50
B. Combustor Metal Loss Rate	55
C. Combustor Deposit Formation Rate	55
D. Exhaust Gas Smoke Density	58
VII. CONCLUSIONS	61
VIII. REFERENCES	63

TABLE OF CONTENTS (Continued)

<u>TABULATIONS</u>	<u>Page</u>
TABLE I - Characteristics of Test Fuels	3
TABLE II - Schedule of Operating Conditions	5
TABLE III - Effect of Fuel Type and Operating Conditions on Combustor Flame Tube Temperatures	52
TABLE IV - Effect of Fuel Type and Operating Pressure on Metal Loss, Deposits and Smoke	56
 <u>ILLUSTRATIONS</u>	
FIGURE 1 - Diagram of Combustor Test Section and Related Piping	4
FIGURE 2 - Schematic Diagram of Spectrophotometer	7
FIGURE 3 - Spectrometer Control Panel and Recorder	9
FIGURE 4 - Upstream View of Spectrophotometer	10
FIGURE 5 - Side View of Spectrophotometer	11
FIGURE 6 - Downstream View of Spectrophotometer	12
FIGURE 7 - Top View of Spectrophotometer	13
FIGURE 8 - Diagram of Laboratory Scale Jet Combustor	15
FIGURE 9 - Monochromator Slit Schedule and Global Emission Spectrum	17
FIGURE 10 - Normal Heptane Flame Emission Spectra (1-5 Microns)	19
FIGURE 11 - Isooctane Flame Emission Spectra (1-5 Microns)	20
FIGURE 12 - Benzene Flame Emission Spectra (1-5 Microns)	21
FIGURE 13 - Toluene Flame Emission Spectra (1-5 Microns)	22
FIGURE 14 - Normal Heptane Flame Emission Spectra (1-5 Microns)	23
FIGURE 15 - Isooctane Flame Emission Spectra (5-15 Microns)	24
FIGURE 16 - Benzene Flame Emission Spectra (5-15 Microns)	25
FIGURE 17 - Toluene Flame Emission Spectra (5-15 Microns)	26
FIGURE 18 - Exhaust Gas Emission Spectra	28

TABLE OF CONTENTS (Continued)

<u>ILLUSTRATIONS</u> (Continued)	<u>Page</u>
FIGURE 19 - Flame Absorption Spectra (1-5 Microns)	29
FIGURE 20 - Flame Absorption Spectra (5-15 Microns)	30
FIGURE 21 - Atomized Fuel Absorption Spectra	31
FIGURE 22 - Air Path Absorption Spectra	33
FIGURE 23 - Open Stationary Nonluminous Flame Emission Spectra	35
FIGURE 24 - Theoretical and Experimental Global Emission Spectra	37
FIGURE 25 - Theoretical Black Body and High Pressure Toluene Flame Emission Spectra	39
FIGURE 26 - Radiation Intensity at 4.4 Microns vs Temperature	41
FIGURE 27 - Radiant Energy Contributed by Various Sources	43
FIGURE 28 - Radiation Intensity vs Position Along Combustor	45
FIGURE 29 - Radiation Intensity vs Operating Condition	46
FIGURE 30 - Radiation Intensity for Extended Combustor Dimensions	47
FIGURE 31 - Transmission Properties of Window Materials	49
FIGURE 32 - Diagram of Combustor Showing Thermocouple Locations	51
FIGURE 33 - Flame Tube Temperature vs Position Along Combustor	53
FIGURE 34 - Flame Tube Temperature vs Operating Condition	54
FIGURE 35 - Flame Tube Metal Loss vs Combustor Pressure	57
FIGURE 36 - Flame Tube Deposits vs Combustor Pressure	59
FIGURE 37 - Exhaust Gas Smoke Density vs Combustor Pressure	60

PHILLIPS PETROLEUM COMPANY

BARTLESVILLE, OKLAHOMA

RADIATION FROM LABORATORY SCALE JET COMBUSTOR FLAMESI. INTRODUCTION

During the bimonthly period of July and August, 1956, our time was devoted largely to analysis and interpretation of the flame radiation program test results, which were obtained under the preceding Contract NOas 52-132-c, Amendment 13.

Since initiating work with Phillips' high pressure combustor test facility, it has been observed that among the more prominent effects of operating pressures in the range of ten to seventeen atmospheres pressure are several related to increased heat transfer from the combustion zone to surrounding metal surfaces. Test results discussed in Reference 1 showed combustor flame tube deposits at such pressures dropping to very low levels, in the face of increased carbon formation shown by exhaust gas smoke density measurements. However, accompanying these deposit reductions at high operating pressures were severe combustor durability problems, manifested by buckling of the flame tubes, distortion of the primary air inlet holes, and burning away of metal from the exposed surfaces.

It was further indicated by measurements of combustor flame tube metal temperatures that both effects, that is, reduced flame tube deposits and increased flame tube failures, may be reflections of hotter metal surfaces. Since the flames with all test fuels, whether paraffinic or aromatic, were brilliantly luminous in appearance at pressures above ten atmospheres, it was believed that these higher surface temperatures were the result of more intense flame radiation. This possibility was explored to a limited extent using a total radiation pyrometer (thermopile type) viewing the flame downstream from the test combustor. The results, though somewhat questionable as to precision, tended to support an explanation of both low deposit rates and high metal burn-off rates on the basis of flame radiation.

Thus it was felt that a more detailed study of the characteristics of the radiant energy emitted from two-inch diameter jet combustor flames might be both worthwhile and timely — in view of industry trends towards relatively high pressure ratio turbojet powerplants. Work done by two other investigators (2, 3) has also shown increasing pressure to cause more intense heat transfer from the flame zone (primary combustion zone) to the surrounding metal walls, using full scale combustor cans at pressures between one and three atmospheres. In both cases the much higher radiation intensities from yellow or luminous flames (containing glowing particles of free carbon as individual radiating centers) compared to that from blue or non-luminous flames was mentioned. It is, of course, known that the formation of free carbon in flames is favored by high operating pressures. Therefore the work covered herein was planned to emphasize realism of the combustion environment, particularly with regards to pressure, with advanced design aircraft powerplants in mind.

It was decided to establish whether the use of Vycor or quartz windows to protect total radiation pick-ups from the high combustor pressures and temperatures (as was done for the work of References 1 and 2 respectively) was permissible from the energy transmission standpoint. That is, is there appreciable radiant energy emitted at wavelengths longer than two or three microns in the infrared region, beyond which Vycor and quartz fail to transmit appreciably? Work discussed in Reference 4 using atmospheric, bunsen burner type flames suggested that this long wave length radiation comprised a large part of the total radiant energy emitted. The experimental program which evolved had the objectives of determining detailed radiant energy-versus-wavelength relationships by the use of spectroscopic instrumentation, for fuels spanning a wide range of hydrocarbon type, at combustor operating conditions representative of (1) ramjet, (2) current turbojet and (3) future turbojet powerplants.

II. TEST PROGRAM

For these studies it was decided to concentrate on pure hydrocarbon test fuels, to insure that differences in flame radiation produced by gross differences in hydrocarbon structure would be clearly evident. Table I lists a number of pertinent characteristics of the four fuels selected -- normal heptane, isooctane, benzene and toluene. All are relatively non-viscous volatile products to minimize, or at least render constant, the effects of liquid atomization and vaporization on carbon formation and, hence, flame radiation.

The basic equipment, that is the test combustor itself and related auxiliaries, was as described in Reference 1 and, more completely, in Reference 5. In brief, the combustor test facility was built around a compressor plant capable of supplying air at mass flow rates up to 2.5 lbs/sec and pressures from 4 to 500 in. Hg abs to a battery of electric resistance heaters, with which combustor inlet temperatures up to 1000 F could be attained. From these the air passed to the combustor inlet piping shown in Figure 4, which also gives the location of the test combustor itself and the stations at which the flame radiation measurements were made. Fuel was introduced into the combustor by pressure atomization through a conventional swirl type nozzle, while air for combustion and cooling entered through holes in the flame tube and nozzle holder. These flame tubes were made from heavy walled (Schedule 40) stainless steel (Type 304) 2-inch pipe to resist distortion and warping in the presence of extreme variation in operating conditions.

The schedule of operating conditions chosen for this work is shown by Table II. Test condition 40 is a combination of low absolute pressure and high inlet air velocity representative to some extent of ramjet type combustion systems -- it was selected as a "base" condition at which all four fuels were expected to burn with blue, smokeless flames. It therefore served to show whether differences might exist between fuels in radiant energy solely of the molecular, or non-luminous, type.

Test condition 150 was chosen to simulate the type of combustion environment provided by current and earlier turbojet engines of relatively low pressure ratio at sea level conditions, or by higher pressure ratio engines at high altitudes. Past observations have shown flames produced under conditions such as this from the two aromatic test fuels to be entirely luminous in appearance, while the two paraffinic test fuels produced semi-luminous flames having both blue and yellow regions.

TABLE I

CHARACTERISTICS OF TEST FUELS

(Handbook Values for Technical Grade Products)

	<u>NORMAL</u> <u>HEPTANE</u>	<u>ISOOCTANE</u>	<u>BENZENE</u>	<u>TOLUENE</u>
Identification Number	A239	A5	A240	A153
Specific Gravity, 60/60F	0.689	0.692	0.834	0.872
ASTM Distillation, F				
Initial Boiling Point	203	205	176	230
50 Percent Evaporated	206	207	176	231
Dry Point	209	208	177	232
Low Heating Value, Btu/lb	19,175	19,065	17,259	17,425
Reid Vapor Pressure, lbs/sq in	1.62	1.71	3.22	1.03
Latent Heat of Vaporization, Btu/lb	156.8	132.2	186.3	177.3
Surface Tension, 80 F, Dynes/cm	17.7	18.9	26.8	25.9
Kinematic Viscosity, 100 F, cs	0.53	0.63	0.60	0.58

PHILLIPS PETROLEUM COMPANY
RESEARCH DIVISION REPORT 1574-54R

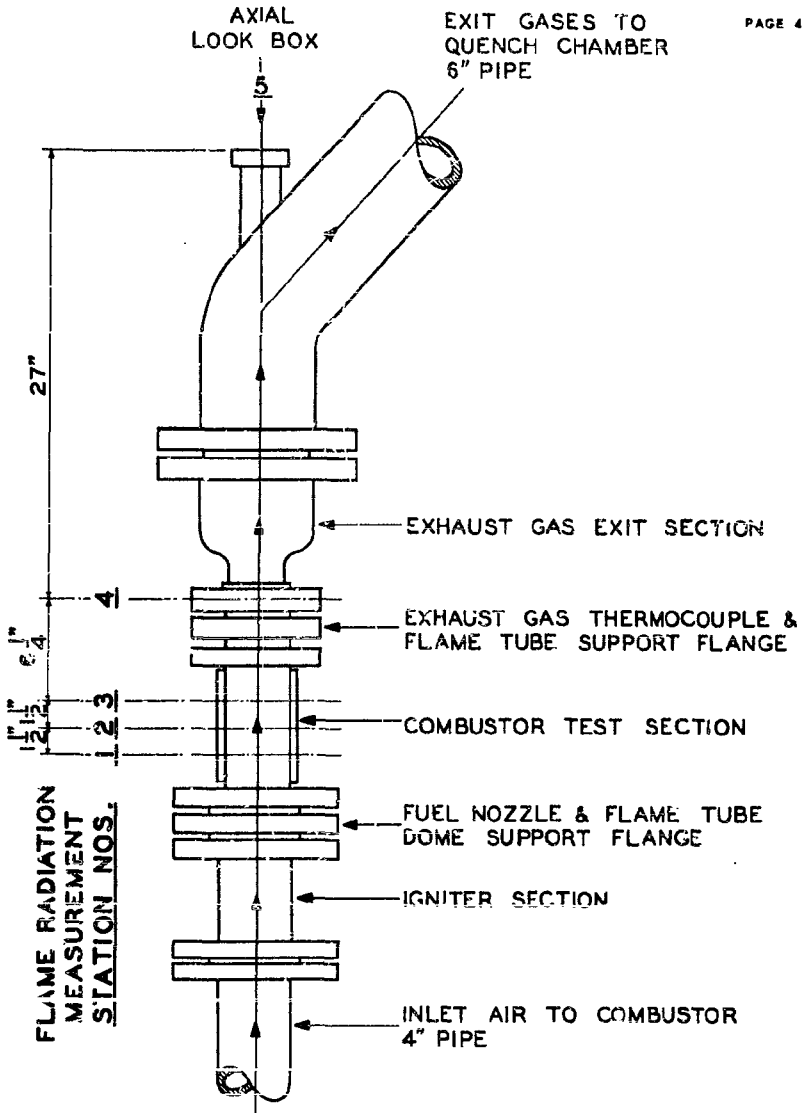


FIGURE 1
DIAGRAM OF COMBUSTOR TEST SECTION AND RELATED PIPING

TABLE II

SCHEDULE OF OPERATING CONDITIONS

<u>Test Condition</u>	<u>40</u>	<u>150</u>	<u>450</u>
<u>Combustion System</u>	Ramjet	Turbojet, Low	Turbojet, High
<u>Environment Simulated</u>		<u>Pressure Ratio</u>	<u>Pressure Ratio</u>
Combustor Pressure, in. hg abs	40	150	450
Combustor Inlet Air Temperature, F	300	400	400
Combustor Inlet Air Velocity, ft/sec	350	100	100
Fuel-Air Ratio, lbs Fuel/lb Air	0.010	0.010	0.010
Mass Air Flow, lbs/sec	0.53	0.50	1.36
Mass Fuel Flow, lbs/hr	19.1	18.0	48.8

Test condition 450 simulated the type of conditions encountered with certain current and future high pressure ratio turbojets, particularly at low altitude conditions. However, it should be mentioned that pressure was the only variable changed here from condition 150, since a corresponding increase in inlet air temperature (desirable for strict realism) was decided against because of doubts concerning the ability of the potassium bromide windows, through which the flame radiation measurements were taken, to withstand temperatures much above 400 F. Inlet velocity, too, was constant for both conditions 150 and 450. A 100 ft./sec velocity was chosen as a reasonably valid compromise between conditions in older, low pressure ratio engines (60 - 80 ft/sec) and those typifying newer, high pressure ratio units (125 - 180 ft/sec).

Fuel-air ratio was maintained constant at the intermediate level of 0.010 for all three test conditions, facilitating interpretation of the radiation data for conditions 150 and 450 on the basis of pressure alone.

III. EXPERIMENTAL SET-UP

The infrared emission and absorption spectra of flames within the laboratory scale jet combustor were the desired spectroscopic information. These spectra were to be obtained with the combustor operating under the conditions described above. The spectroscopic equipment available was a Perkin-Elmer 12B spectrophotometer converted to a 12C instrument. This conversion consisted of changing the spectrophotometer from d-c operation to a-c operation. The change permitted the use of the more modern a-c amplifying system used on present day Perkin-Elmer equipment and provided a convenient means for obtaining both the emission and absorption spectra of the flames. The spectrometer was mounted on the laboratory scale jet combustor to form the jet-combustor spectrophotometer.

A schematic diagram of the jet-combustor spectrophotometer is shown in Figure 2. The two-inch diameter flame tube within the combustor test section had 1/4-inch diameter air inlet holes through which the spectra were obtained. To obtain absorption spectra a first image of the Globar source was projected by mirror M1 and lens L1 (aperture 3/4-inch) at the center of the combustor. An image of this first image was projected by lens L2 (aperture 1/2-inch) onto the slit of the monochromator. The radiation from the Globar was modulated at 13 cps by the light chopper C1 with chopper C2 set in the open position. This modulated radiation was dispersed by the monochromator and detected by the thermocouple receiver. The 13 cycle output from the thermocouple was selectively amplified. This amplified signal was synchronously rectified by breaker points attached to the shaft of the chopper C1. The resulting d-c signal, proportional to the amount of radiation falling on the thermocouple, was recorded. Thus, radiation arising between the chopper C1 and the thermocouple receiver was rejected unless it happened to be modulated at 13 cps and had the proper phase. Therefore, the modulated radiation reaching the thermocouple was derived from the Globar source and passed through the flame in the combustor permitting absorption measurements to be made. Spectra were obtained by continuously varying the wavelength passed by the monochromator over the spectral region desired.

Emission spectra were obtained by setting C1 in the closed position and modulating the radiation leaving the combustion chamber by means of chopper C2. The amplified signal from the detector was synchronously rectified by breaker

PHILLIPS PETROLEUM COMPANY
RESEARCH DIVISION REPORT 1524-568

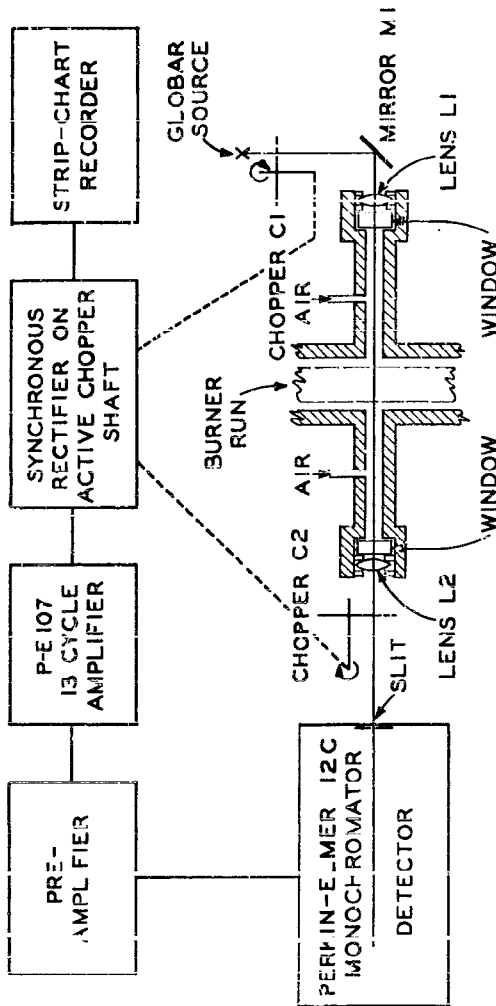


FIGURE 2
SCHEMATIC DIAGRAM OF SPECTROPHOTOMETER

points attached to the shaft of C2. In this case, only radiation originating between C1 and C2, in the flame tube, was modulated and was thus recorded. With this arrangement the emission or absorption spectra could be obtained by activating the proper chopper and breaker points.

The lenses L1 and L2 were made of potassium bromide with a focal length of 5.33 inches. The lenses were separated from the combustion chamber by plates of potassium bromide one centimeter thick. The plates were sealed by means of plastic O-rings to fittings attached to the combustion chamber. In order to cool the potassium bromide plates and to prevent deposition of water, oil, carbon, etc., on the windows, dry air was injected between the window and the combustion chamber as shown in the diagram.

A. Spectrophotometer Details

In the interest of safety and operator convenience it was required that the spectrophotometer be operated by means of controls which were located outside the test-cell. Therefore, a 25 foot cable was used between the controls and the equipment located inside the test-cell. Figure 3 is a photograph of the control, amplifying, and recording system standing alongside the test-cell control panel, just outside the test-cell.

In Figure 3 the top panel contained the control circuitry for the two chopper-breaker switch assemblies, scanning drive, and slit drive. The selector switch at the left switched the amplifier output to utilize the rectifier breaker points associated with the particular light chopper being used (i.e., absorption or emission). It also switched the standard signal voltage through the standard signal breaker point associated with the light chopper. The left hand toggle switch energized the light chopper motor desired. The center toggle switch position determined the direction of rotation of the monochromator scanning drive motor. The spectra were obtained by scanning from short to long wavelength. The 3-position toggle switch on the right controlled the direction of rotation of the monochromator slit drive motor to open, close or stop the slit.

The recorder was a slightly modified Minncapclis-Honeywell 10 millivolt recorder. The panel immediately above the recorder was the control panel for the Perkin-Elmer Model 107 amplifier. The panel immediately below the recorder contained, left to right, the watt-meter measuring the power consumed by the Global source, the source power switch, the Variac control for the source voltage, the power switch, and the a-c line voltage meter. The bottom panel contained the start and stop push button switches for the monochromator scanning motor along with the pen and chart activation switches. Except for the selector switches and motor reversing switches in the top panel all the circuitry and controls in Figure 3 were standard with Perkin-Elmer equipment.

Figures 4 through 7 show various photographic views of the spectrophotometer attached to the combustor test section. Other equipment in the test-cell has been obliterated from the background merely to make the photographs readable.

Figure 4 is an up-stream view of the combustor run taken from the exhaust end. Water-cooled plates, 1, carrying the chopper-breaker assemblies and the Global source were supported on the combustor test section by two pieces

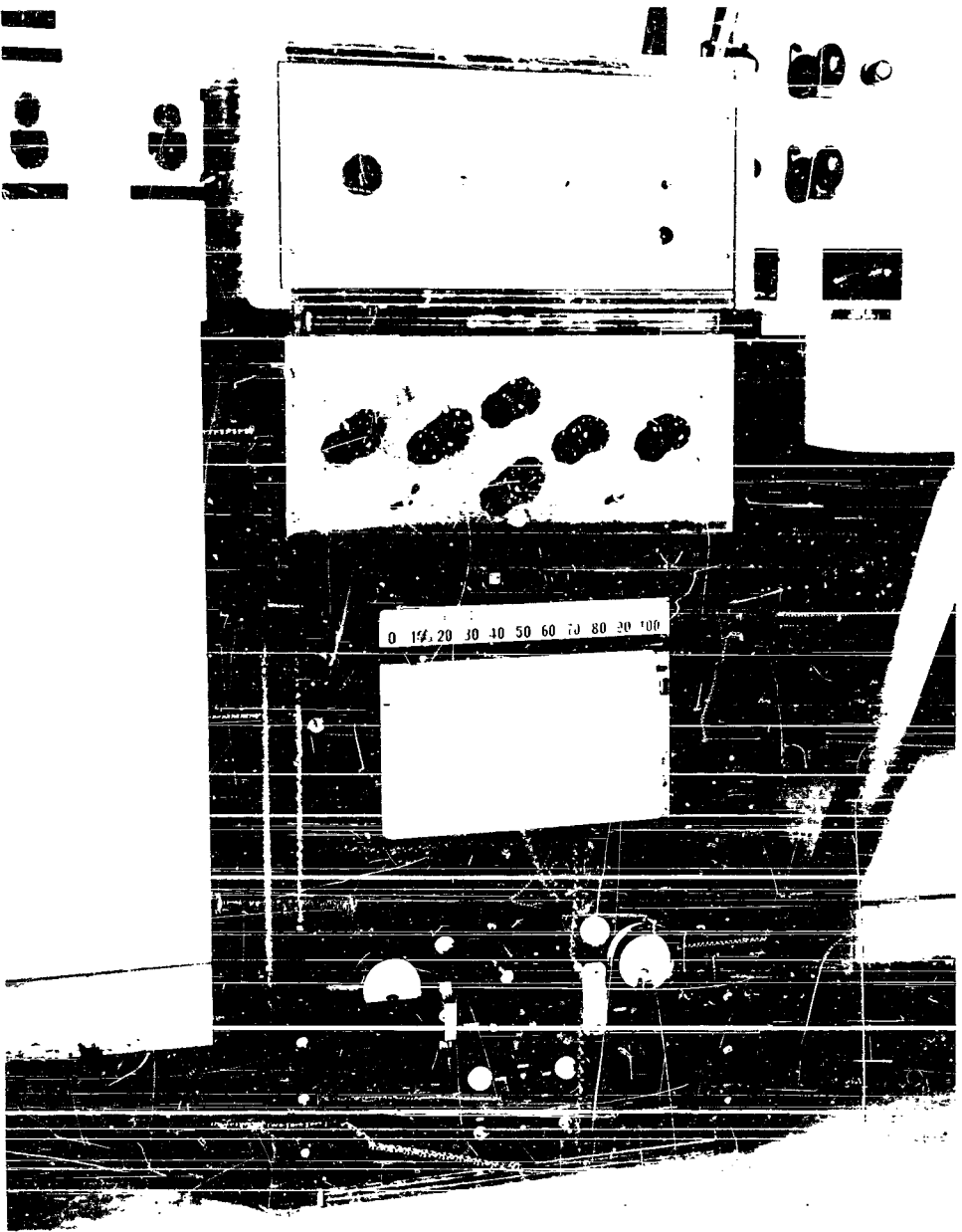


FIGURE 3
SPECTROMETER CONTROL PANEL AND RECORDER

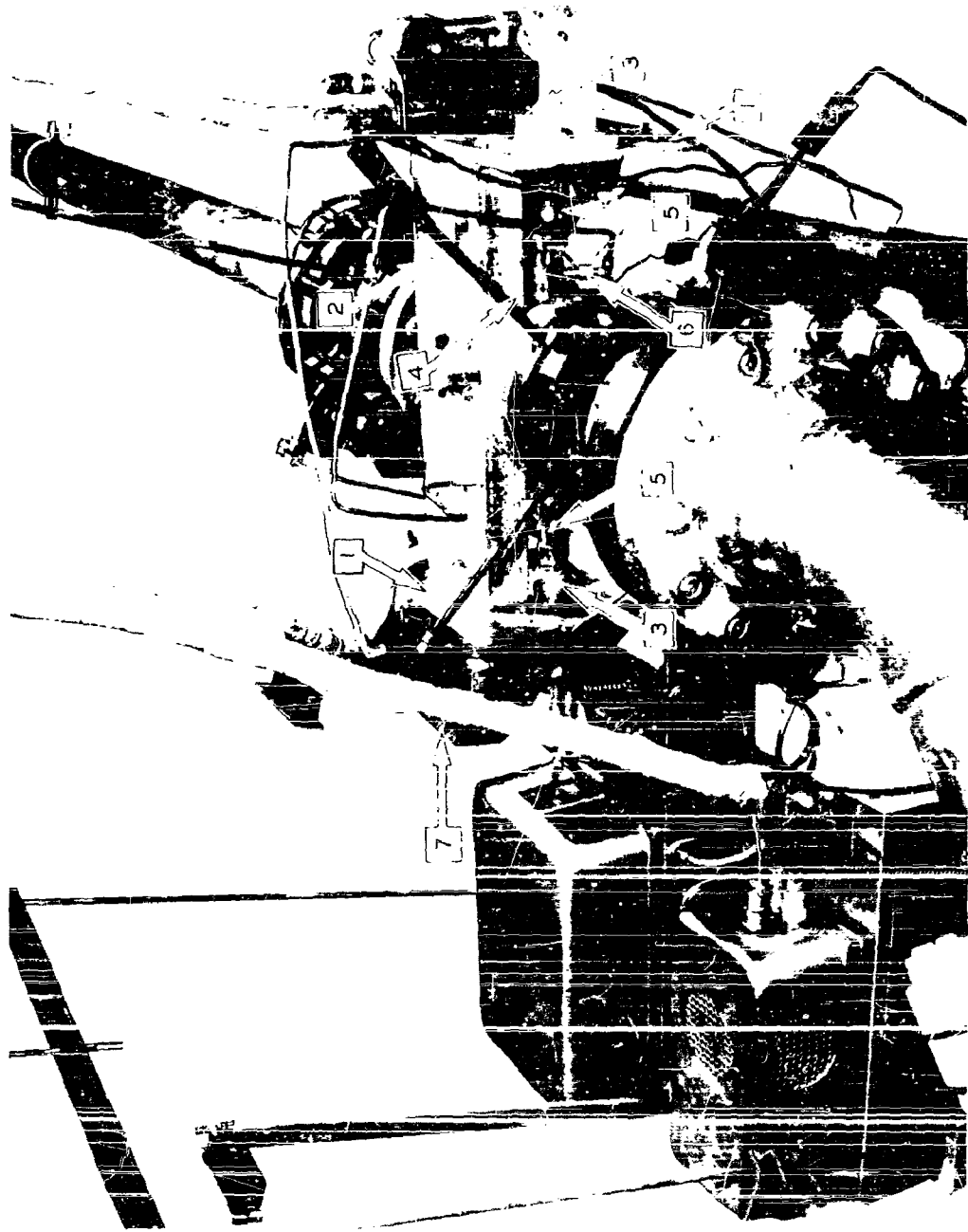


FIGURE 4
UPSTREAM VIEW OF SPECTROPHOTOMETER

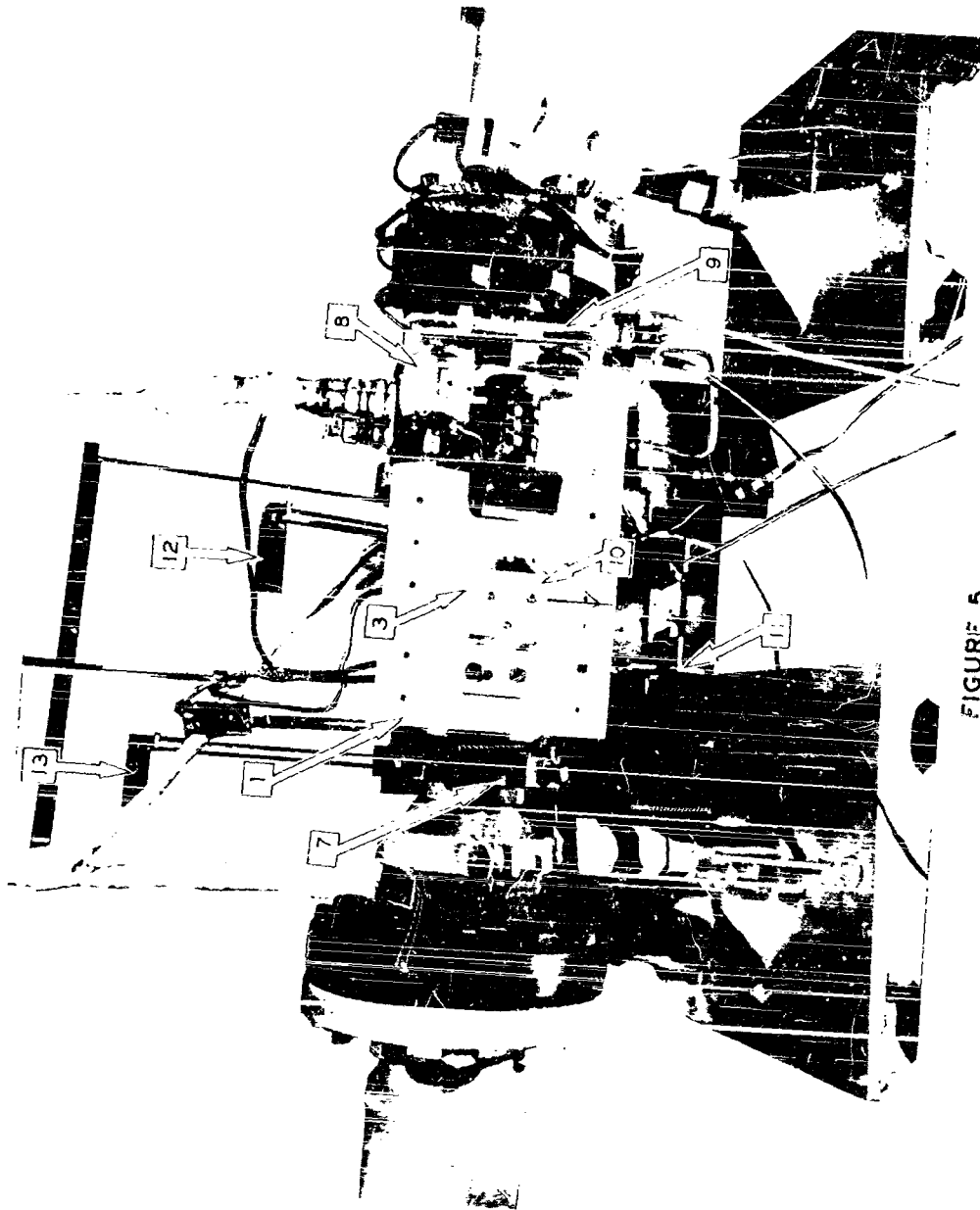


FIGURE 5
SIDE VIEW OF SPECTROPHOTOMETER

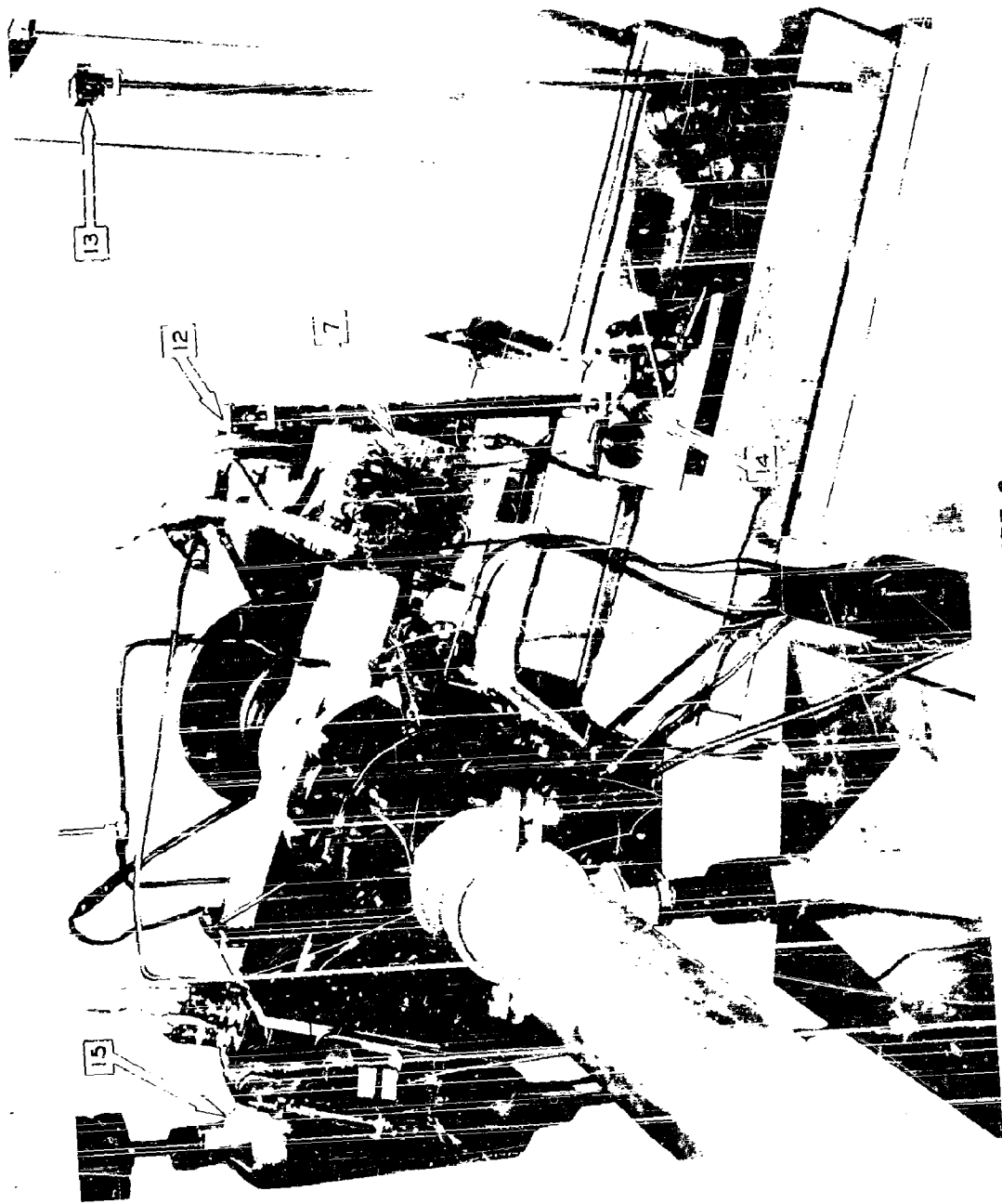


FIGURE 6

PHILLIPS PETROLEUM COMPANY
RESEARCH DIVISION REPORT 1326-56R

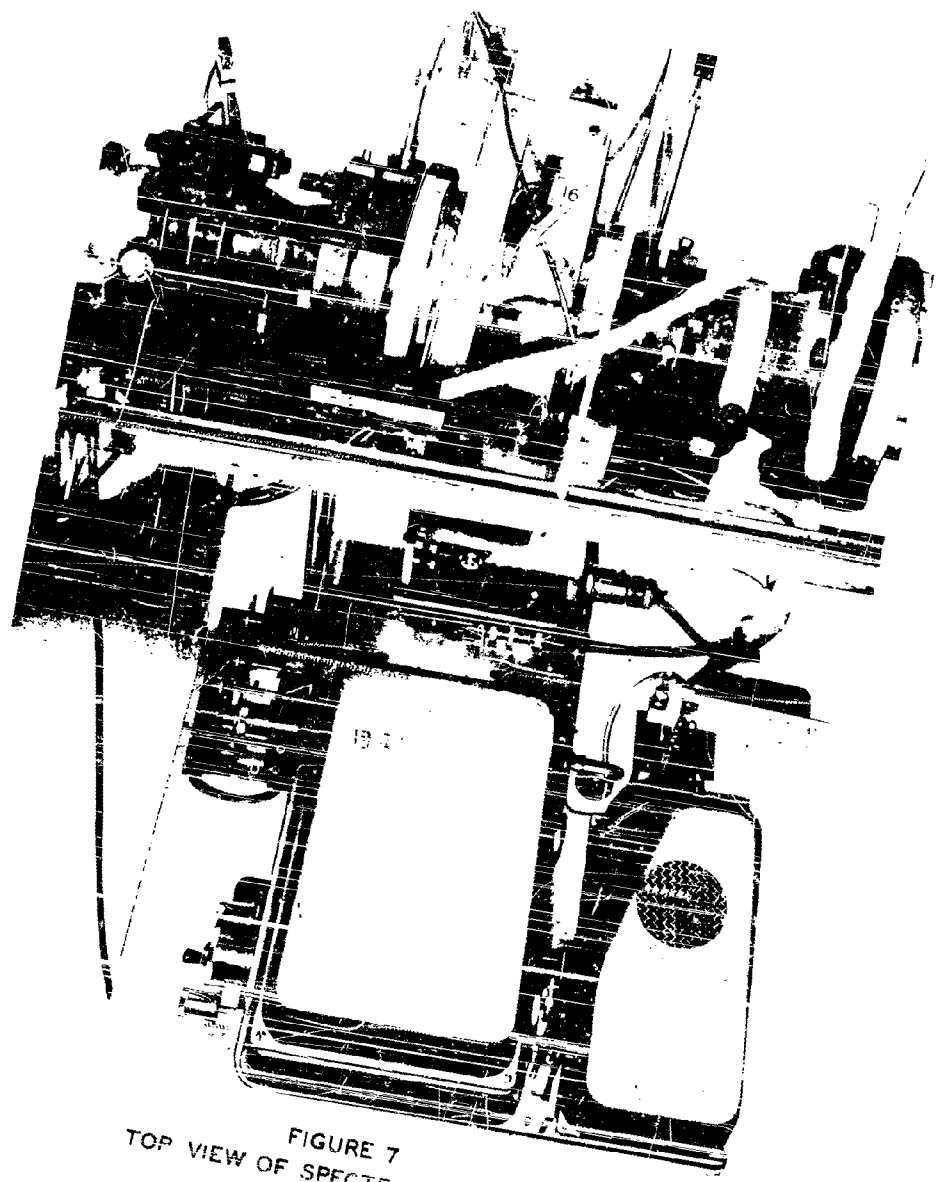


FIGURE 7
TOP VIEW OF SPECTROPHOTOMETER

of angle iron, 2. The lens-window holders, 3, projected through the water cooled plates. These lens-window holders were supported from the combustor test section by nipples, 4, and gate valves, 5. The dry purge air was injected into the nipples by the injectors, 6. The spectrophotometer was mounted at a 15 degree angle to the horizontal to conform with the flange arrangement on the combustor test section. The light chopper and rectifier breaker assembly used for emission measurements was enclosed in box 7.

Figure 5 is a view, perpendicular to the combustor run, as seen through the observation window in the test-cell control panel. The light chopper, G1, for obtaining absorption spectra, its associated rectifier breaker points, and drive motor, 8, were located on the water cooled plate, 1. The radiation from within the Globar housing, 9, was reflected by mirror M1, 10, into the combustor section through the lenses in the lens-window holder, 3. The optical path was folded at this point to prevent obstruction of the walk-aisle alongside the combustor run.

Immediately below the water-cooled plate may be seen part of the mounting bracket, 11, used to rigidly attach one end of the monochromator to the combustor test section. The other end of the monochromator was hung from the ceiling by a sling. This permitted the monochromator to move with the combustor test section, maintaining proper alignment with the test section and those parts of the spectrophotometer attached to it. With changes in operating conditions, motion of the combustor run was significant, due to changes in temperature and consequent expansion and distortion of the exhaust system.

Two Veeder-Root counters are visible in Figure 5. Counter 12 indicated the width of the monochromator slit in millimeters. Counter 13 indicated the rotational position of the wavelength scanning lead screw in units of the standard Perkin-Elmer wavelength drum. These counters permitted reading the slit width and wavelength drum position through the control panel observation window without entering the test cell.

Figure 6 is a view looking downstream along the combustor run. This view shows the gear train, 14, and motor for controlling the monochromator slit width. At the left is the purge air drying tower, 15, containing 15 pounds of Drierite.

Figure 7 is a view from above the combustor run. The axis of the monochromator was not perpendicular to the axis of the combustor. This was done in order to conserve the radiant energy available at 15 microns by using the refracting edge of the sodium chloride prism. The monochromator was thermostated at 100 F. This low temperature was possible because the test-cell was adequately ventilated and this work was done during cold weather. This view also shows one of the two aligning pins, 16, inserted into the combustor test section to insure that the flame tube did not move with respect to the housing.

B. Combustor Details

A sketch of the flame tube in the combustor test section is shown in Figure 8. The transverse spectroscopic observations on the flames were made through 1/4-inch air inlet holes located diametrically across the tube. The stations numbered 1, 2, and 3 indicate the locations used along the axis of the

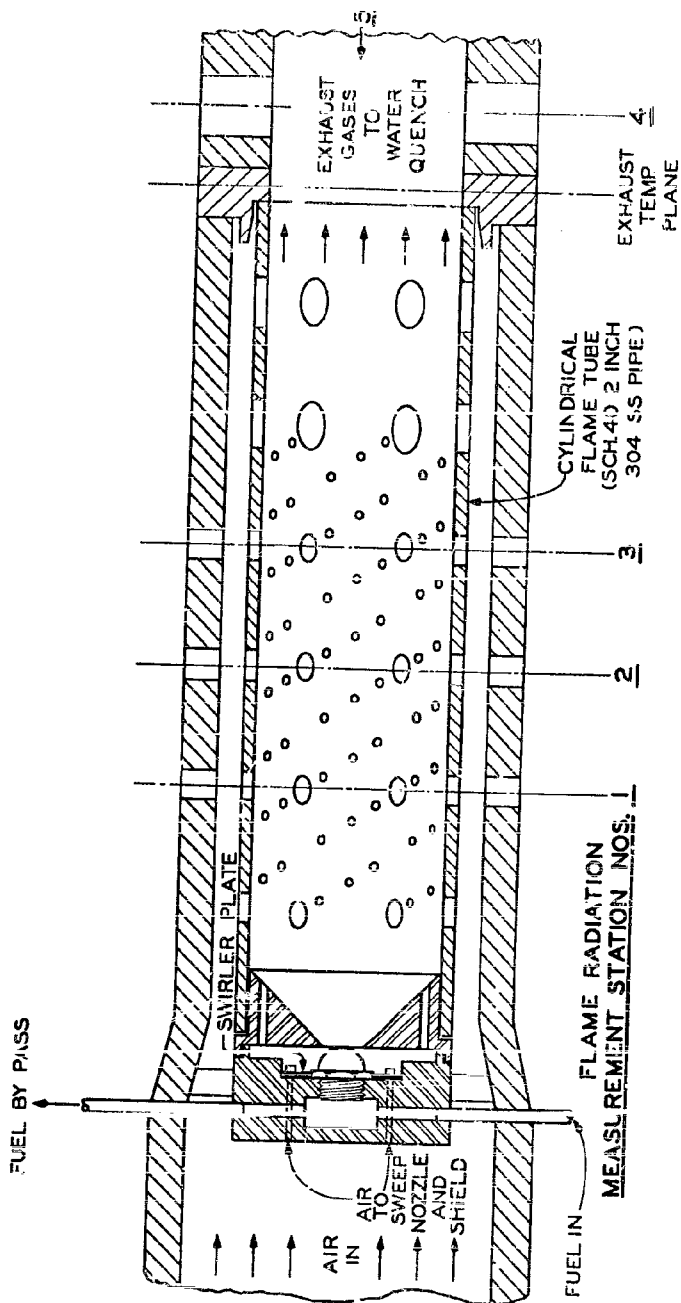


FIGURE 8
DIAGRAM OF LABORATORY SCALE JET COMBUSTOR

flame tube. These numbers will be used throughout this report to designate these observation stations. Transverse observations were also made downstream from the flame quench holes in the combustor exhaust gas stream at the station numbered 4. These observations were made through holes in flange 17 shown in Figure 5.

Axial observations from the exhaust end were made through an observation window in the exhaust elbow approximately 4.5 inches downstream from the flame tube. This station is designated as station 5. An unobstructed axial view of the flame was obtained from this station.

The purge air used at stations 1, 2, and 3 was obtained ahead of the flow-control throttling valve but after the flow rate metering orifice plate. This gave sufficient pressure drop to maintain a positive flow of air through the purge air injectors between the potassium bromide windows and the combustor. This air was a part of the air metered to the combustor, therefore, it was included in the fuel-air ratio. The purge air used at stations 4 and 5 was obtained ahead of the orifice plate. Therefore, it was not a part of the air metered to the combustor and was not included in the fuel-air ratio.

Emission and absorption spectra were obtained at stations 1, 2, 3, and 4 but only the emission spectra was obtainable at 5. All four fuels described in Table I were investigated for each of these observation stations along the combustor under the three conditions specified in Table II.

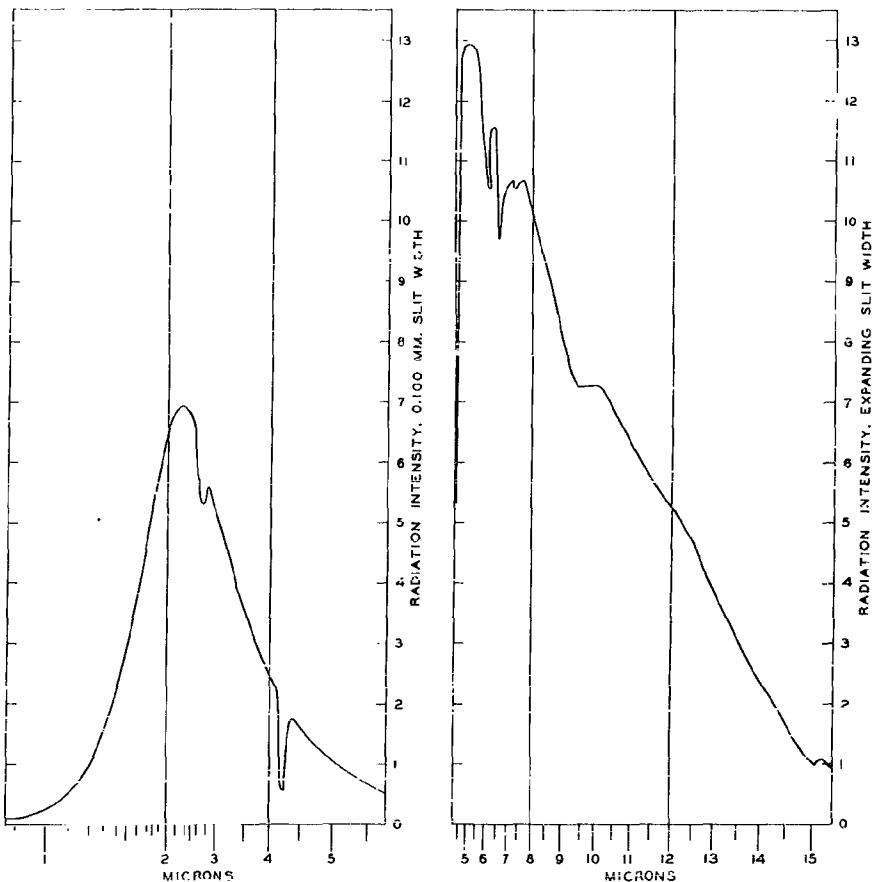
IV. INFRARED SPECTRAL MEASUREMENTS

The infrared spectral data obtained with the spectrophotometer are described below. This consists of the raw lateroignospectrophotometric and posteroignospectrophotometric data. The former were obtained at stations 1, 2, 3, and 4, the latter at station 5. Some of the details concerned with obtaining the data, the reliability of the data, and methods of reducing the data to usable form are also discussed below.

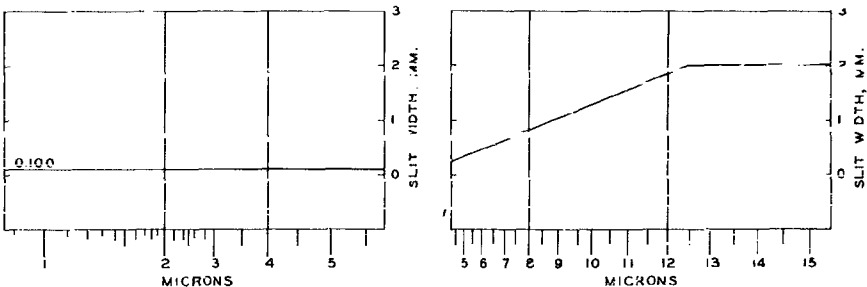
A. Emission Spectra

The short wavelength spectral region, 0.9 to 5.5 microns, was scanned with a constant monochromator slit width (usually 0.100 millimeters). To save taking of data and maintain reasonable recorder deflections for non-luminous portion of a long wavelength spectrum, 4 to 12.5 microns, was scanned with constantly increasing monochromator slit width. The slit width varied linearly from 0.22 millimeter at 4 microns to 2.0 millimeters at 12.5 microns. The slit width was held constant at 2.0 millimeters from 12.5 to 15 microns. The slit was continuously opened according to the prescribed schedule by using synchronous motors for driving the monochromator wavelength scanning mechanism and cam for the monochromator slits. The slit width schedule is shown in the lower part of Figure 9. The upper curve illustrates the effect of this slit schedule on a familiar Globar radiation curve. The Globar was operated at 2700 K in the combustor spectrophotometer described above. The same Globar operating conditions were used in obtaining the infrared absorption spectra to be discussed later.

STATION 2



GLOBAR EMISSION



SLIT SCHEDULE

FIGURE 9
MONOCHROMATOR SLIT SCHEDULE AND GLOBAR EMISSION SPECTRUM

Some inconsistencies appeared in the spectra due to optical alignment difficulties and flame tube distortion. The stability of the alignment was improved during the course of taking the data so that all of the data do not reflect the same degree of reproducibility. In addition to changes in the alignment reliability some of the data are influenced by the fact that the collection of foreign matter on the potassium bromide windows was progressively reduced during the early part of this work. The deposition problems were overcome by adequate drying of the purge air and by using the proper start-up procedures. Since this work was something of a survey project some accuracy was sacrificed in the interest of decreasing combustor operating time and of covering a larger number of combustor conditions and fuels.

Figures 10 through 13 are short wavelength emission spectra of normal heptane, isooctane, benzene, and toluene flames, respectively. Figures 14 through 17 are the corresponding long wavelength spectra. The combustor operating conditions, 40, 150, and 450, are indicated on the spectra. These spectra were obtained at the observation stations 1, 2, 3, and 5 reading from left to right as labeled at the top of the figures.

The short wavelength spectra at positions 1, 2, and 3 were obtained at a constant slit width, 0.100 millimeter. At position 5 the slit width was 0.070 millimeter. In order to present the spectra on a uniform intensity scale the information from station 5 was normalized to a slit width of 0.100 millimeter and corrections applied for the length of slit illuminated and for the optical aperture of the viewing arrangement. This intensity scale is the same as that used in Figure 9. The normalization to a 0.100 millimeter slit was made by assuming that at these slit widths the recorder deflection was proportional to the square of the slit width. The lumped corrections for the lengths of the slit illuminated and the optical aperture were obtained empirically, as follows.

Since for any one fuel at test conditions 150 and 450 the 4.4 micron carbon dioxide peak emission at stations 1, 2, 3, does not change greatly, the peak intensity for station 5 was assumed to be the same. This assumption is based on the observation that the transverse absorption of the flames at this peak wavelength is essentially complete, thus, the emissivity is essentially one. Therefore, for a particular temperature, in this case the same flame, the peak intensity will be constant. The same correction factor obtained thusly, $1/3$, was used on all the station 5 data. Except for this $1/3$ factor applied to the station 5 data the data were transcribed directly from the recorder traces taking into consideration only the changes in amplifier gain and/or slit width used to keep the recorder deflection on scale.

No evidence of abnormal radiation patterns, other than extensions of the black body type of radiation, were noted in the visible region down to 0.5 microns. Therefore, the spectra were not plotted for wavelengths shorter than 0.9 microns.

The variation in the 4.4 micron peak intensities for the station 1, 2, and 3, conditions 150 and 450, and the station 5, condition 150, spectra is probably a good measure of the reproducibility of the alignment and other instrumental factors. Variations in flame characteristics will account for some other variations.

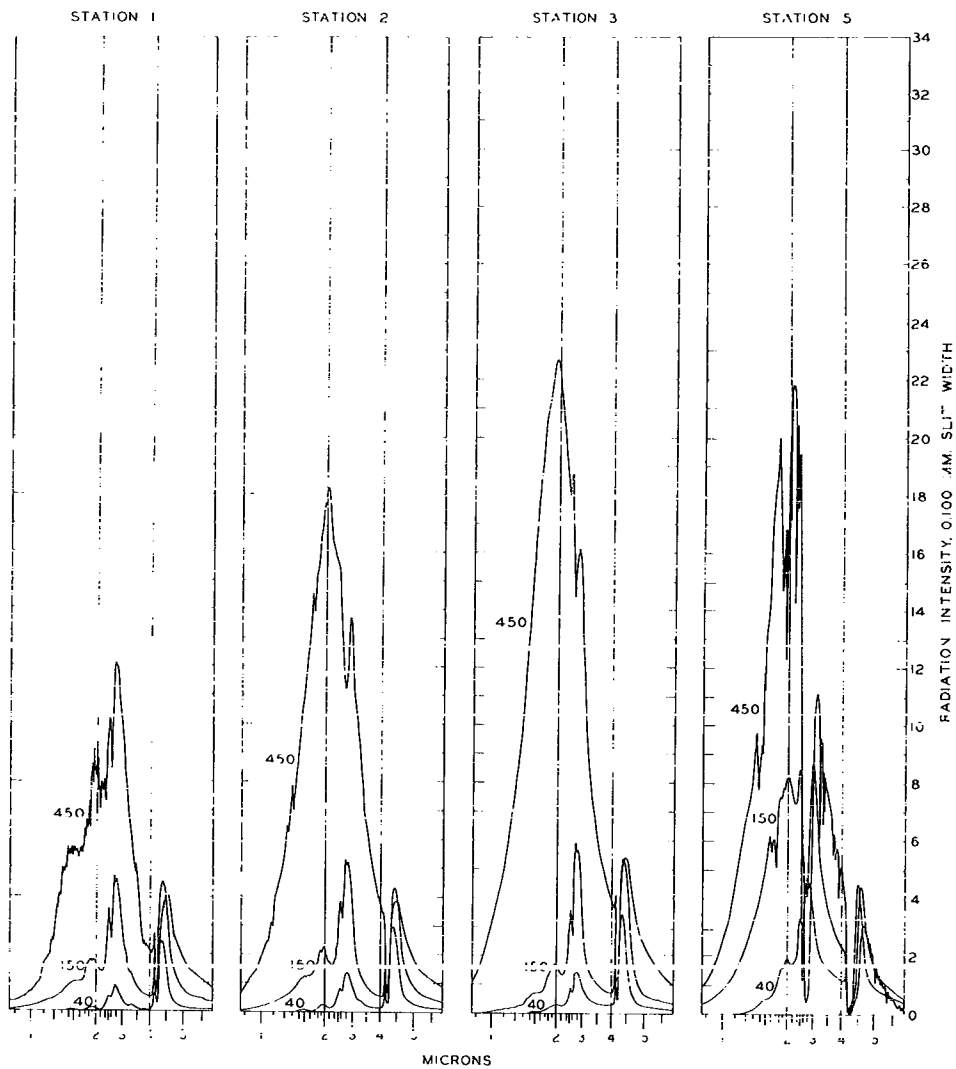


FIGURE 10
NORMAL HEPTANE FLAME EMISSION SPECTRA (1-5 MICRONS)

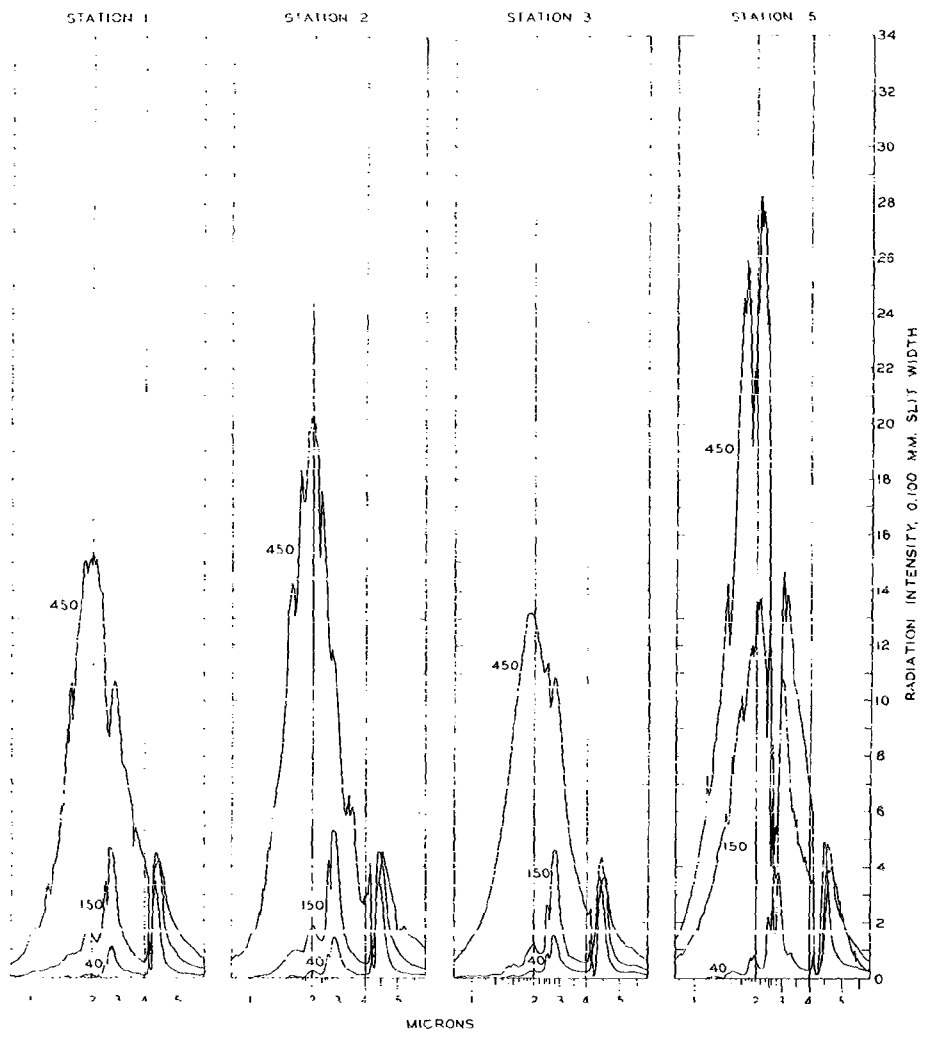


FIGURE 11
ISOCTANE FLAME EMISSION SPECTRA (1-5 MICRONS)

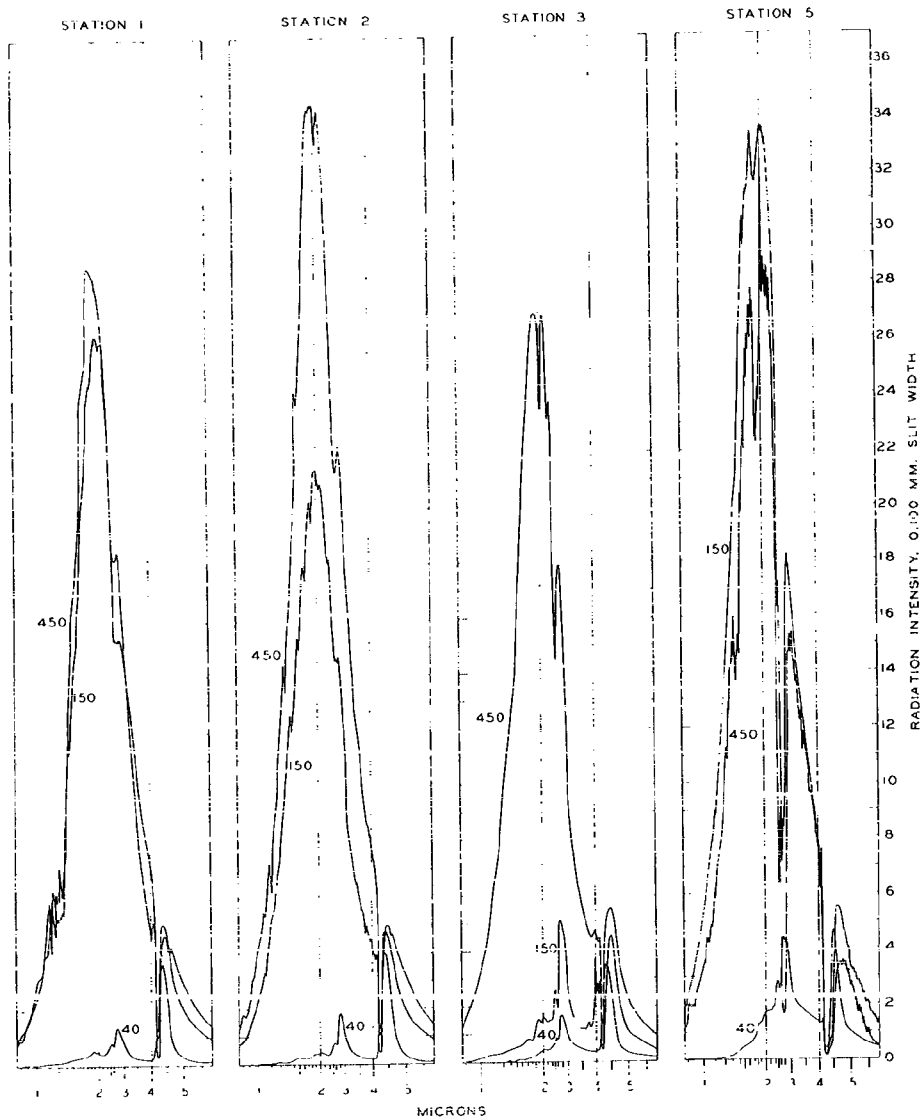


FIGURE 12
BENZENE FLAME EMISSION SPECTRA (1-5 MICRONS)

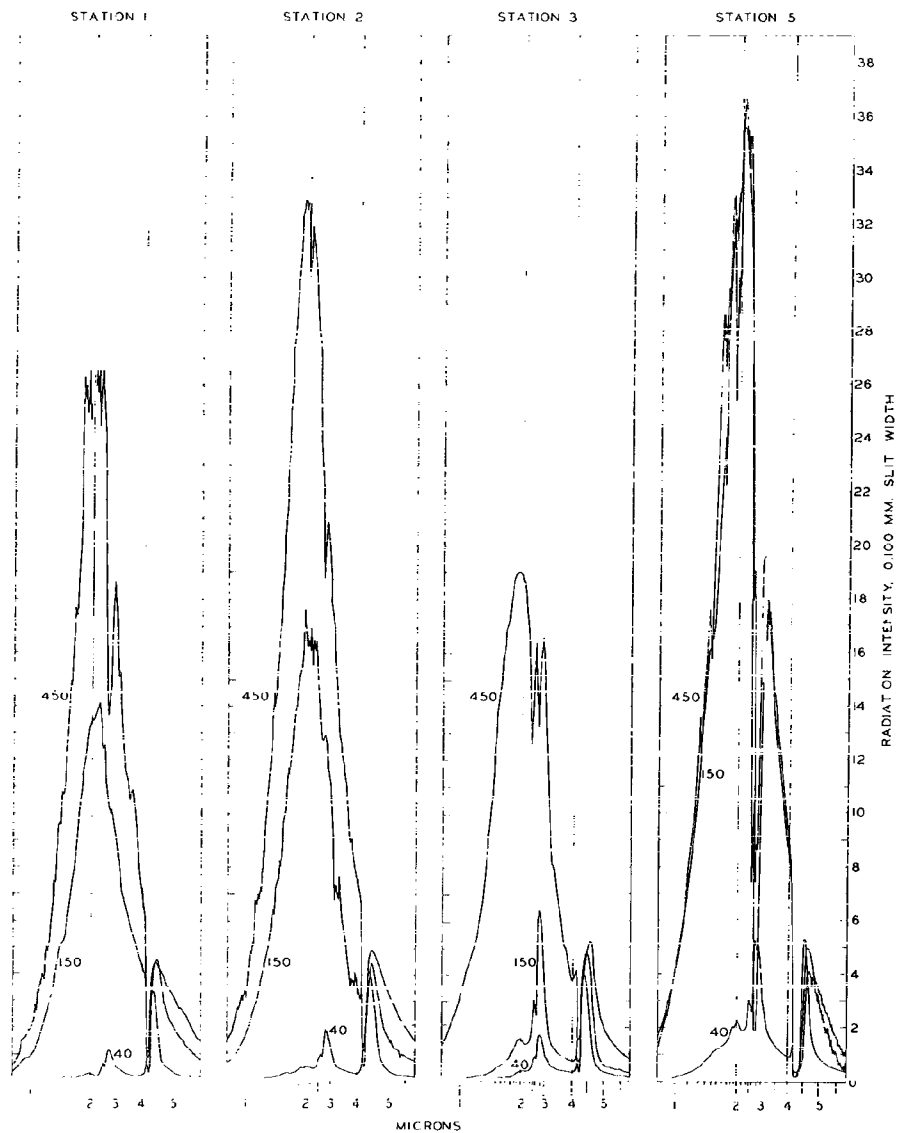


FIGURE 13
TOLUENE FLAME EMISSION SPECTRA (1-5 MICRONS)

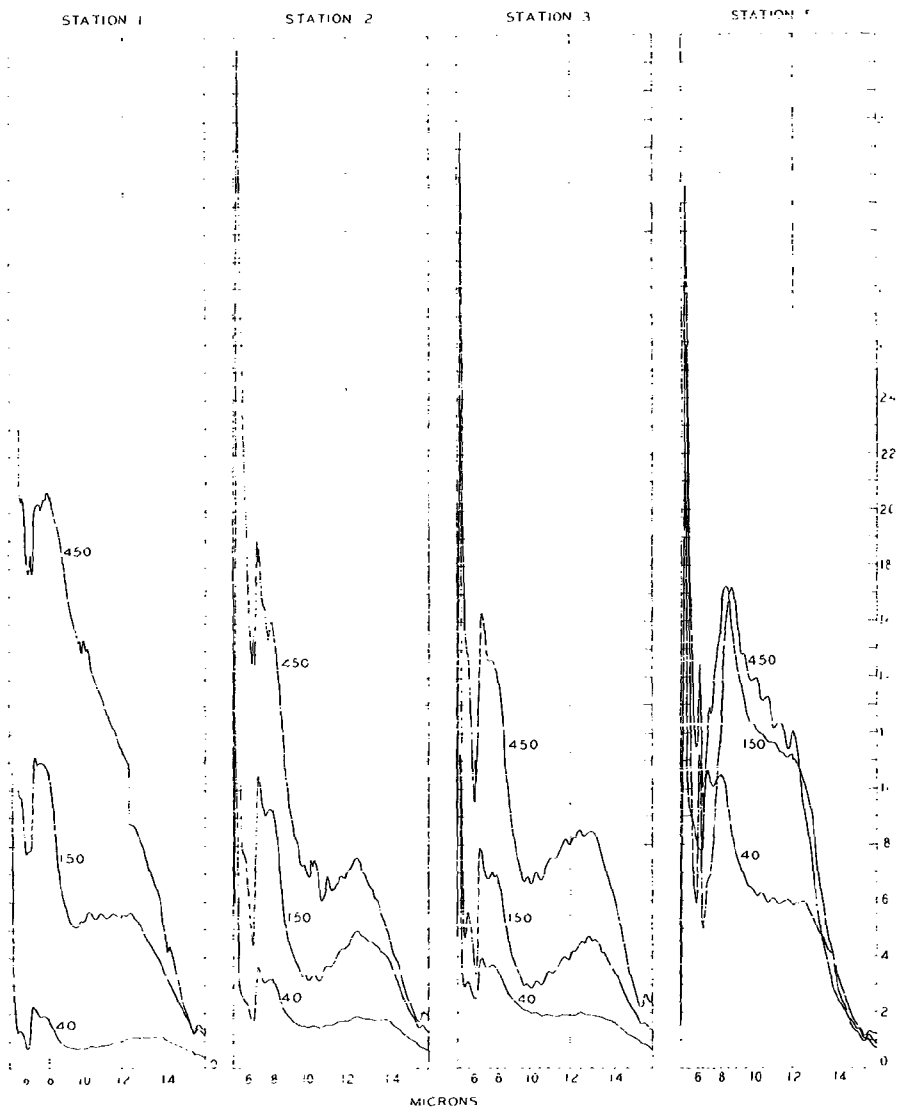


FIGURE 14
 NORMAL HEPTANE FLAME EMISSION SPECTRA (5-15 MICRONS)

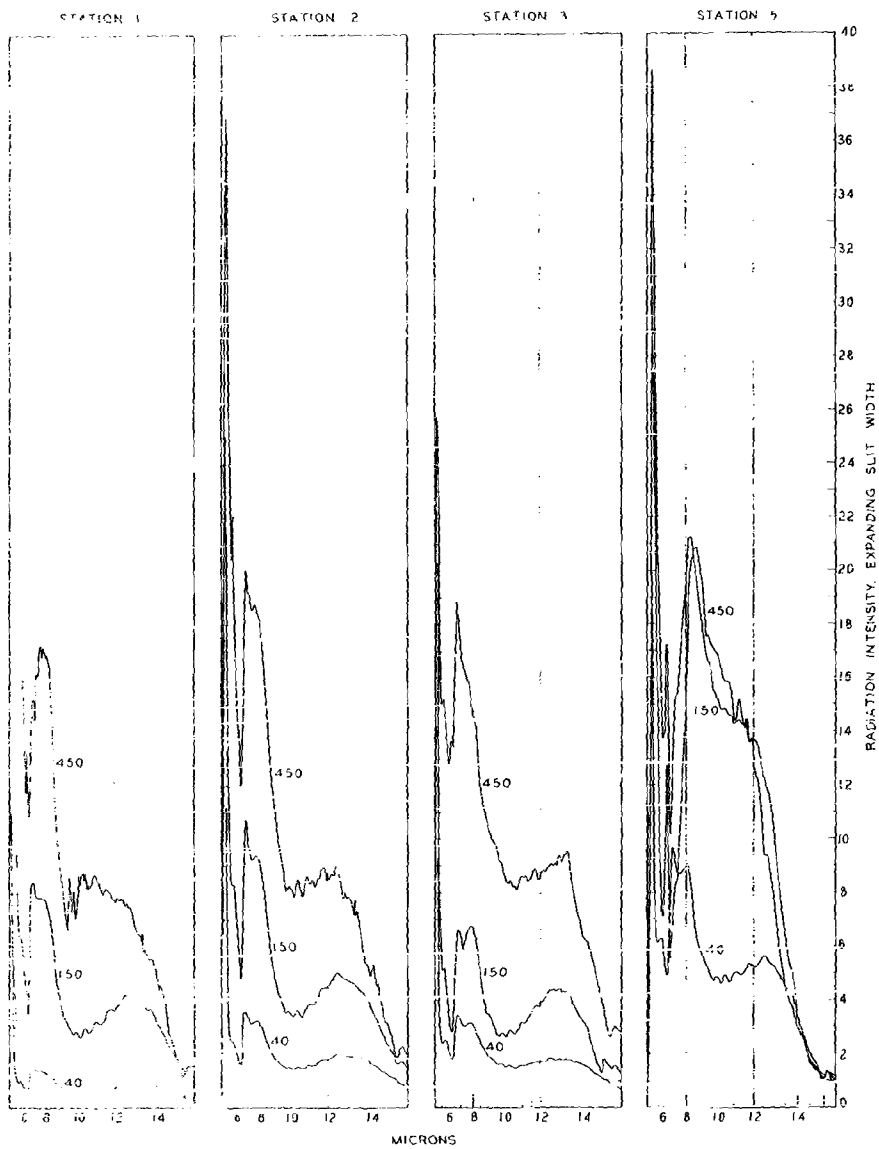


FIGURE 15
ISOOCTANE FLAME EMISSION SPECTRA (5-15 MICRONS)

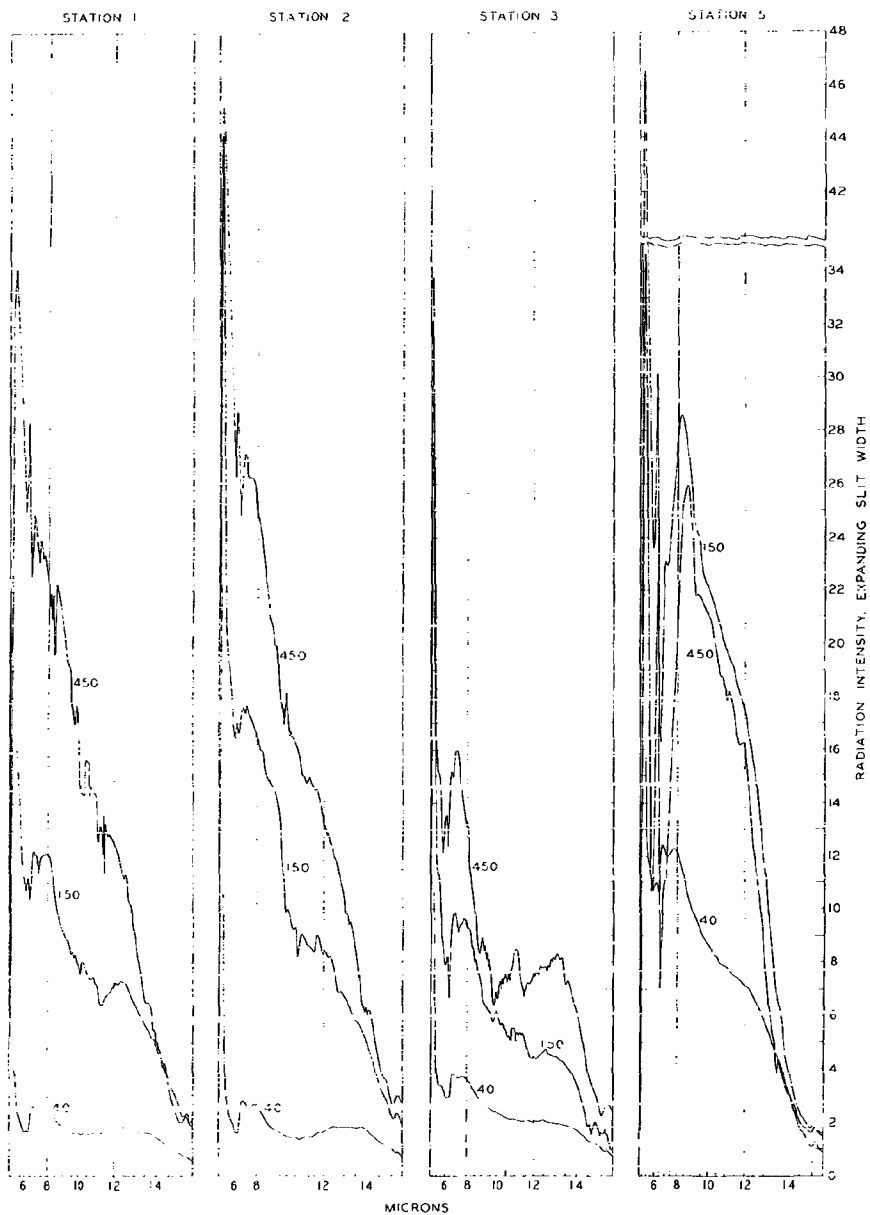


FIGURE 16
 BENZENE FLAME EMISSION SPECTRA (5-15 MICRONS)

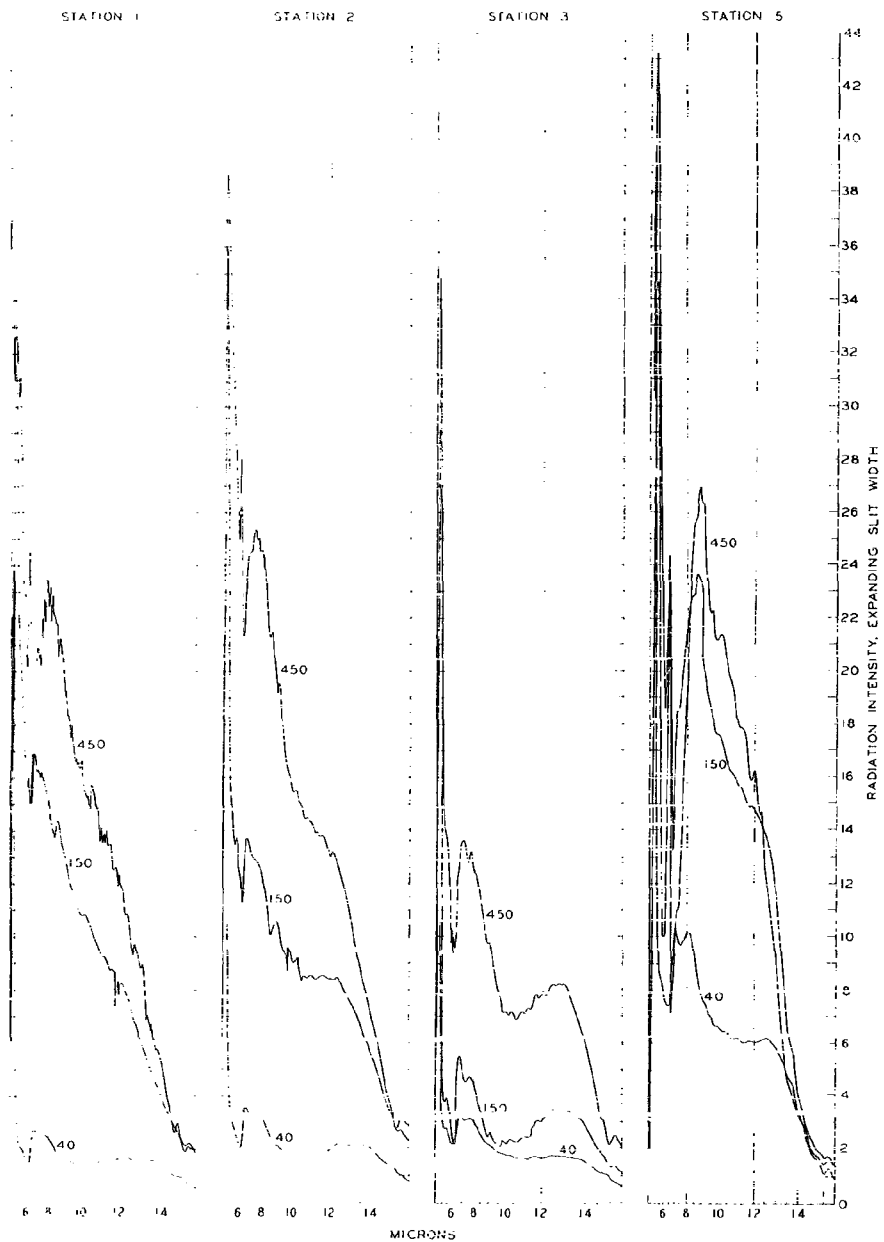


FIGURE 17
TOLUENE FLAME EMISSION SPECTRA (5-15 MICRONS)

The long wavelength spectra were scanned at twice the speed used for the short wavelengths. The slit schedule shown in Figure 9 was used for all the long wavelength spectra. The same factor of 1/3 discussed above for slit illumination and optical aperture corrections was used in plotting the long wavelength station 5 spectra. Again the same intensity scale was used in Figures 14 through 17 as in Figures 9 through 13.

The short wavelength emission spectra at station 4 were obtained with slit widths of 0.100 and 0.140 millimeters. The information transcribed from the recorder chart was normalized to a slit width of 0.100 millimeters. The long wavelength spectra were obtained with the slit schedule in Figure 9. The effective length of the monochromator slit illuminated at station 4 was somewhat greater than at stations 1, 2, and 3. However, the data were not corrected for this factor since the intensity of radiation was so low. The emission spectra for station 4 are shown in Figure 18.

B. Absorption Spectra

The short and long wavelength flame absorption spectra are shown in Figures 19 and 20, respectively. These spectra were obtained by comparing the Global energy curve with a fire in the combustor to the energy with no fire in the combustor. The slit width schedule in Figure 9 was used. The spectra for stations 1, 2, 3, and 4 are arranged from left to right. The spectra from top to bottom are for normal heptane, isooctane, benzene, and toluene. The spectra for test conditions 40, 150, and 450 are indicated on the individual curves.

It will be noted in Figure 9 that the energy distribution was such that the absorption spectra at wavelengths shorter than one micron, or longer than 14 microns, meant little because of the small amount of energy available. Likewise the absorption on the short wavelength side of the 4.4 micron carbon dioxide absorption band was somewhat indeterminate because of the strong carbon dioxide atmospheric absorption. Likewise the absorption in the 2.6, 6 to 7.5 and 15 micron regions was influenced by changes in the water and carbon dioxide absorption in the optical path outside the flame.

The details of the condition 450 spectra where the average per cent transmission was low, below 50 per cent, were rather meaningless since in some cases the signal to noise ratio was less than one. The "noisiness" of the radiation transmitted through the flames appeared to increase with the average absorptivity and luminosity. In general, the energy transmitted by the condition 40 flame was quite steady, noise level of the order of one per cent, condition 150 flame, 5 per cent, the condition 450 flame up to 100 per cent. In the case of emission the noise was never larger than a few per cent of the signal. These noise effects are presumably tied up with the turbulence and density of incandescent material in the flame. Flames having a high spectroscopic noise level were visually "noisy" with considerable fluctuation in the visual intensity, particularly at stations 1 and 2.

Figure 21 shows the absorption spectra of the four vaporized fuels at 450 inches of mercury combustor pressure, as observed at station 2. The raw fuel was injected into the combustor in exactly the same manner as it was in the flame studies except there was no flame. The fuel and air flow rates were those used

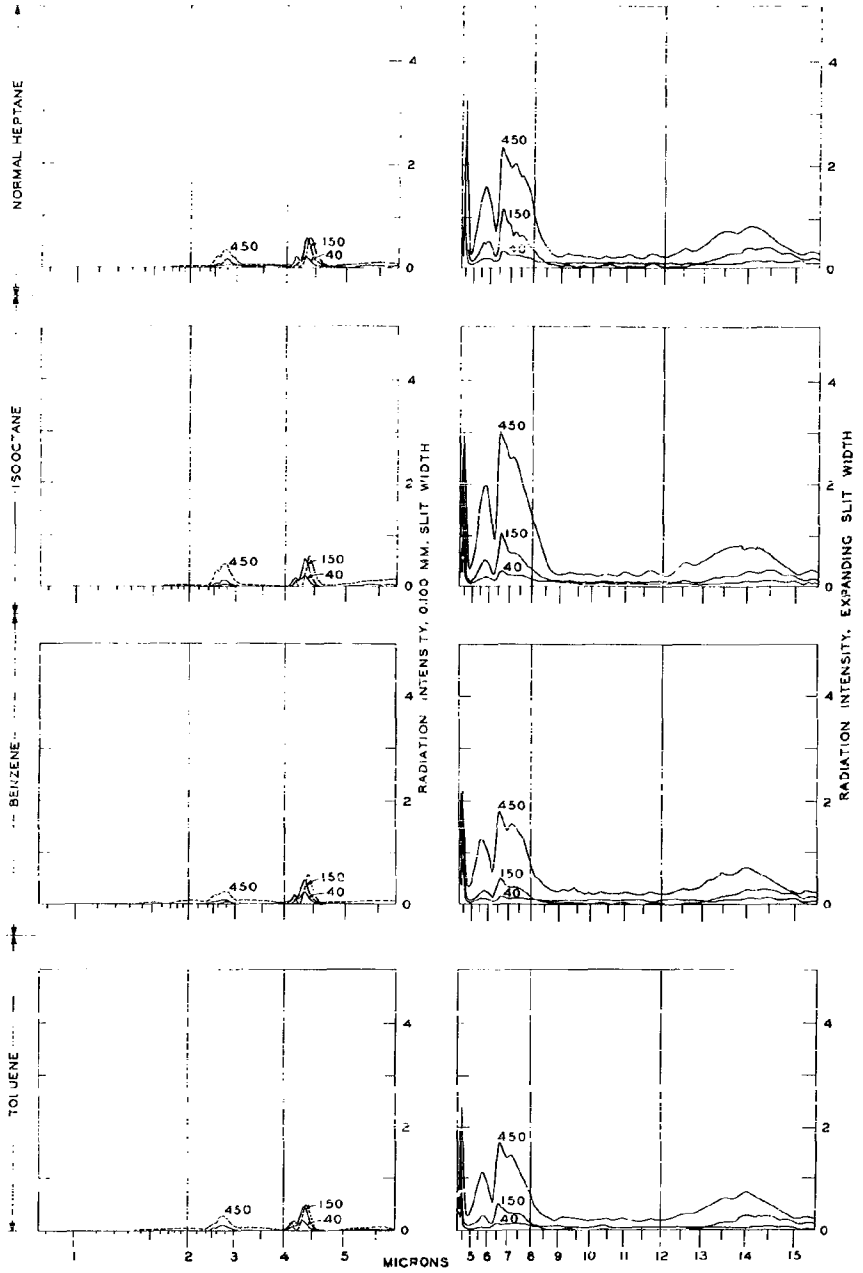


FIGURE 18
EXHAUST GAS EMISSION SPECTRA

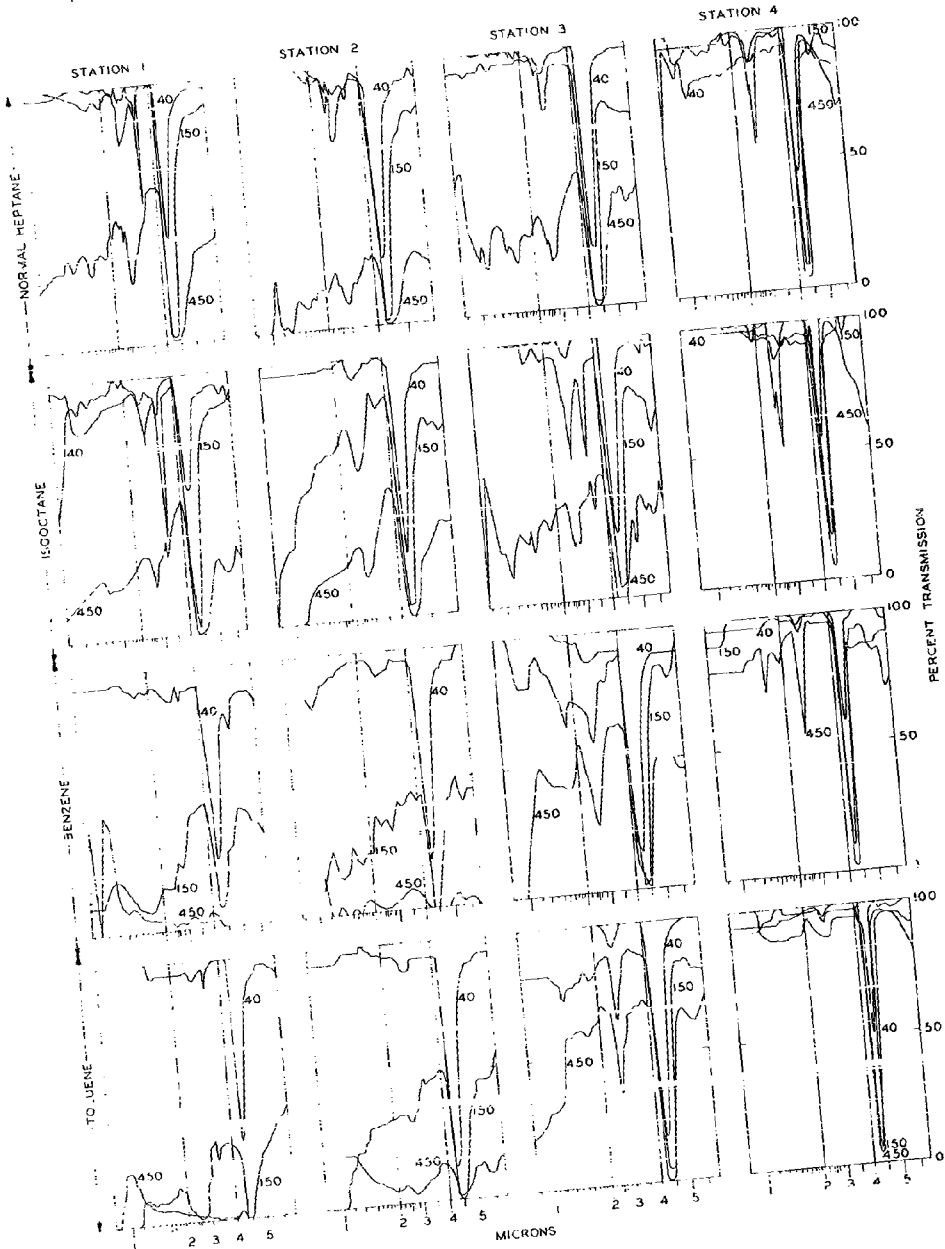


FIGURE 19
FLAME ABSORPTION SPECTRA (1-5 MICRONS)

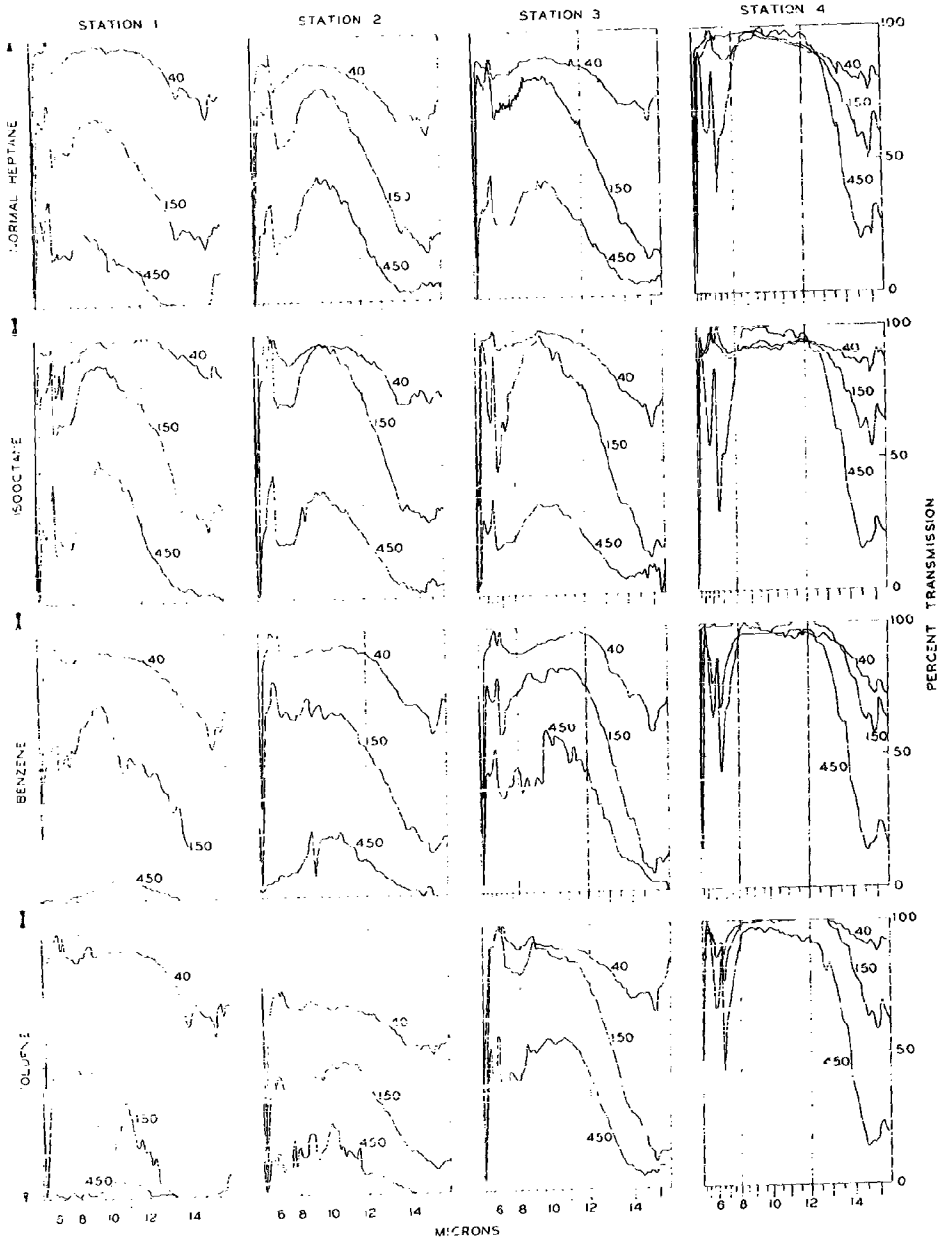


FIGURE 20
FLAME ABSORPTION SPECTRA (5-15 MICRONS)

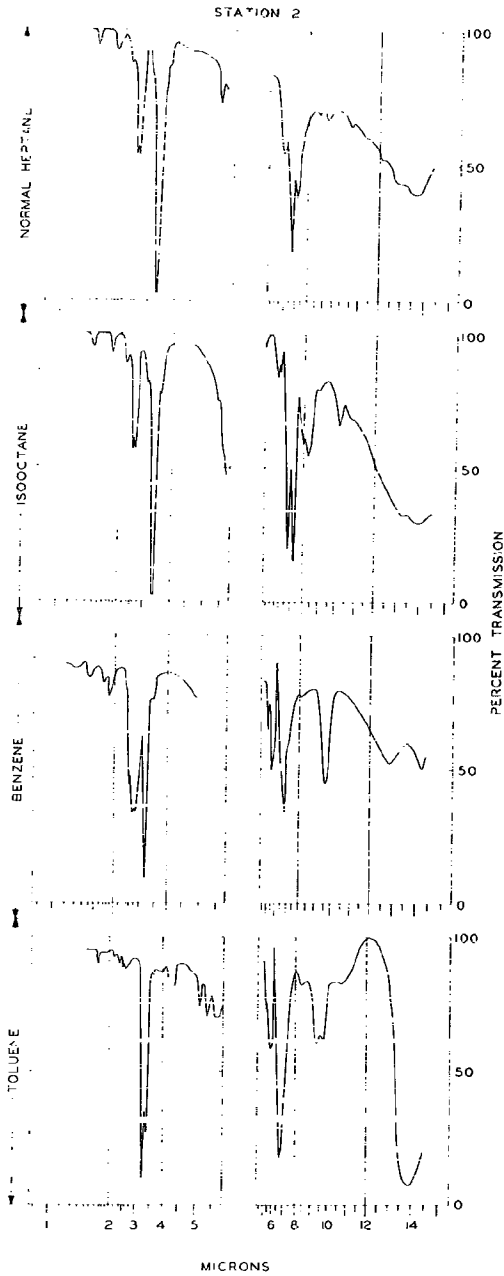


FIGURE 21
ATCMIZED FUEL ABSORPTION SPECTRA

for test condition 450. The inlet air temperature was dropped to 350 F. There are some doubts about the validity of these spectra in the 2.6 to 3 and 5.5 to 6.7 micron regions. These doubts arise because these spectra were obtained before the deposition of foreign matter, particularly water, on the potassium bromide windows was eliminated.

Figure 22 shows the absorption spectra of the water and carbon dioxide in the complete optical system, combustor included, with 40 and 450 inches of mercury air pressure in the combustor. These spectra were obtained by comparing a smooth Globar emission curve, simulating low water or carbon dioxide absorption, to the experimental curve. The smoothing was done in those spectral regions in which an increase in combustor pressure gave a significant decrease in transmission, namely, at 1.9, 2.6, 4.3, 6, and 15 microns. It will be noted from these curves that the approximately 20 inches between the potassium bromide plates contained a large part of the effective atmospheric absorbing materials at 450 inches of mercury pressure (15 atmospheres).

V. DISCUSSION

A. Infrared Spectra

Inspection of Figures 10 through 17 indicates that the experimental flames may be classified into two groups. One group in which molecular (band) type radiation predominates and another group in which black body (continuous) type of radiation predominates. Such a grouping agrees with the visual flame characteristics and the designations non-luminous and luminous, respectively. If more combustor conditions are subsequently investigated more precise nomenclature will be needed. The table below summarizes this information for the fuels and operating conditions used in this work.

<u>Test Fuel</u>	<u>Test Condition</u>		
	<u>40</u>	<u>150</u>	<u>450</u>
Normal Heptane	non-luminous	non-luminous	luminous
Isocetane	"	"	"
Benzene	"	luminous	"
Toluene	"	"	"

In the non-luminous flame spectra, the molecular bands centered at 1.4, 1.9, 2.9, and 7 microns will be recognized as the familiar water vibrational emission bands. There may be some contribution from carbon dioxide at 2.7 microns. Such contribution can be evaluated by studying the spectrum of a carbon monoxide flame. The band in the 4 to 5 micron region was due to carbon dioxide vibrational emission. The carbon dioxide emission in the 15 micron region was not obvious. The shape of these vibrational emission bands was influenced to a large degree by the absorption due to water and carbon dioxide and the air path in the optical train. The absorption at 1.4 and 1.9 microns was due to water, at 2.6 to water and carbon dioxide, at 4.3 to carbon dioxide, at 6.5 to water, and at 15 microns to carbon dioxide. These absorption bands were particularly evident in the station 5 spectra since the radiation traverses about 45 inches of exhaust gases and air at the same pressure as the combustor.

STATION 2

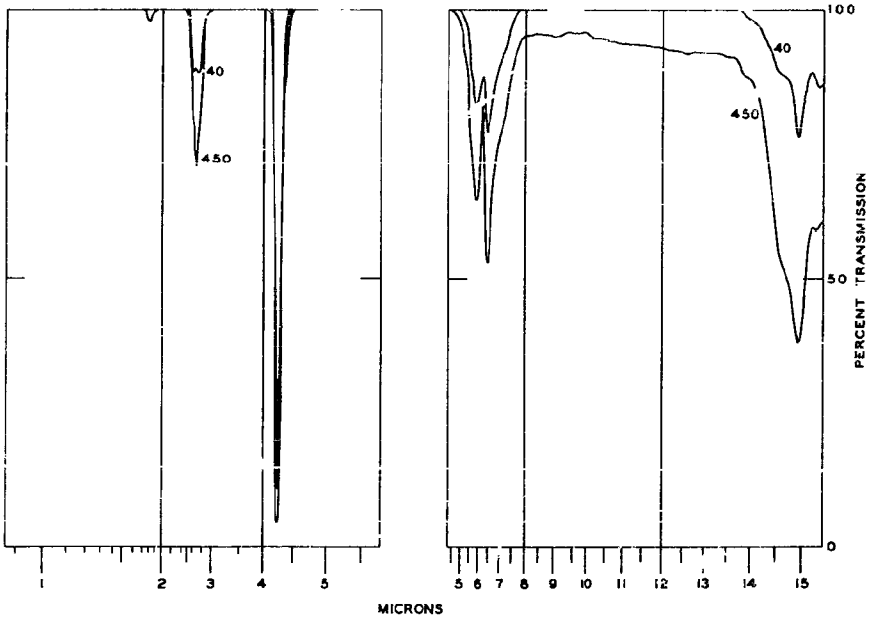


FIGURE 22
AIR PATH ABSORPTION SPECTRA

In the 9 to 13 micron region there appeared to be some coherent structure in the emission curves for both the non-luminous and luminous flames. In the light of some atmospheric pressure methane-air flame radiation studies made by Bell and co-workers (6), these bands may be attributed to water emission. The upper part of Figure 23 is a tracing of Bell's data. Part of these data were obtained at somewhat higher resolution than used in our study. The detailed structure shown in the 6 to 15 micron region has been attributed by Bell to water rotational emission. Such rotational emission arises from two sources. At flame temperatures higher rotational levels are excited than at ambient temperatures. Therefore, the 6 micron water vibrational band will have extended rotational structure. Further, the higher level pure rotational lines will extend into this region from the 20 micron region.

Superimposed on this high resolution curve is a dotted curve. This dotted curve is a visual integration which shows what this curve might look like at the resolution used in the high pressure work. There may be considerable prejudice in this integration; however, it serves as a basis for comparison. The lower part of the Figure 23 is a reproduction of a natural gas-air flame spectrum obtained while preparing the spectrophotometric equipment for the jet combustor investigation. The resolution used here is comparable to that used in the jet combustor work. The monochromator slit widths used are indicated on the curve. The natural gas-air flame was produced in the standard Globar housing that is normally used on a laboratory Perkin-Elmer spectrophotometer. A screen was placed just below the opening in the side of the Globar housing and natural gas (96 per cent hydrocarbon) was injected into the housing from below. The gas was ignited above the screen.

It will be seen on inspection that the details of this low resolution spectrum correlate very well with the dotted curve above. Further, these details correspond to those noted in the 9 to 13 micron region of the jet combustor flame spectra. In the station 5, condition 450, spectra the sense of some of these details is reversed. This arises since with the long column of exhaust gases in the optical path the absorption due to the exhaust gases predominates over the emission. It should be possible to determine whether the increase in emission from 10 to 13 microns is due to water, carbon dioxide, or stripped carbon chain emission by studying the spectra of hydrogen and carbon monoxide flames in atmospheric pressure burners.

One characteristic of a molecular flame emission band is that the wavelength distribution does not correspond to that of the atmospheric absorption. A large part of the emitted radiation appears at longer wavelengths than the atmospheric absorption bands. This may be explained by the fact that the emitting gas is at a higher temperature than the atmospheric absorbing gas. At elevated temperatures the population of the energy states of the molecules is different from that at lower temperatures. The wavelengths of the emission or absorption resulting from transitions between the higher energy states will not coincide exactly with the transitions between the two lowest states. This situation arises because, in general, the molecule is an anharmonic oscillator rather than a harmonic one. The correspondence between the molecular flame emission wavelength distribution and the flame absorption distribution can be seen by inspection of Figures 10 through 20. Since the anharmonicity should increase at higher energy states the flame absorption and emission bands should broaden toward longer wavelengths as the flame temperature is increased. This effect is also evident

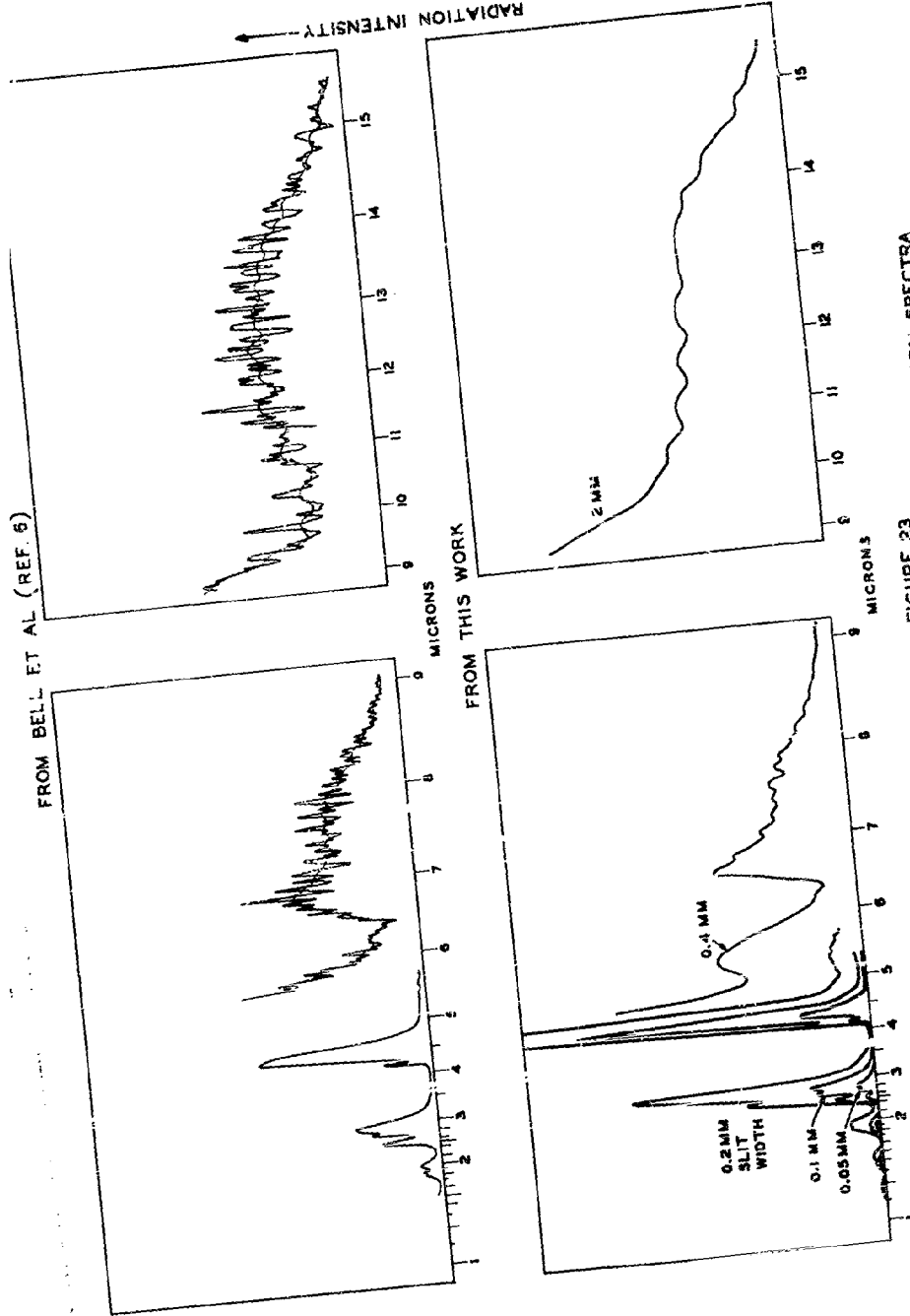


FIGURE 23
OPEN STATIONARY NON LUMINOUS FLAME EMISSION SPECTRA

FROM BELL ET AL (REF. 6)

FROM THIS WORK

if the atmospheric absorption of carbon dioxide at 4.3 microns in the station 1, 2, and 3 emission spectra is compared with the hot exhaust gas absorption in the station 5 emission spectra. Also a comparison of the flame absorption spectra at stations 1, 2, and 3 with the cooler station 4 absorption and the atmospheric absorption shows the same type broadening of the absorption band with temperature.

The spectra of the non-luminous flames show a small background of continuous radiation while in the luminous flame spectra the continuous radiation obscures molecular radiation. In the cases of intermediate luminosity molecular radiation peaks are superimposed on the continuous background. The absorption curves show that in the regions of strong molecular emission the absorptivity is higher than the background. As the luminosity of the flame increases, as evidenced by the increased intensity of the continuous radiation, the molecular bands become less pronounced. It will be noted that, for those flames where the average absorption is nearly complete the continuous radiation at 4.4 microns is no more intense than the molecular radiation under less luminous conditions. Therefore, for the central portion of this band the emissivity is essentially one in the two inch diameter combustor at pressures above 150 inches of mercury. That is, the radiation intensity at this wavelength is equal to that of a black body operating at the temperature of the flame.

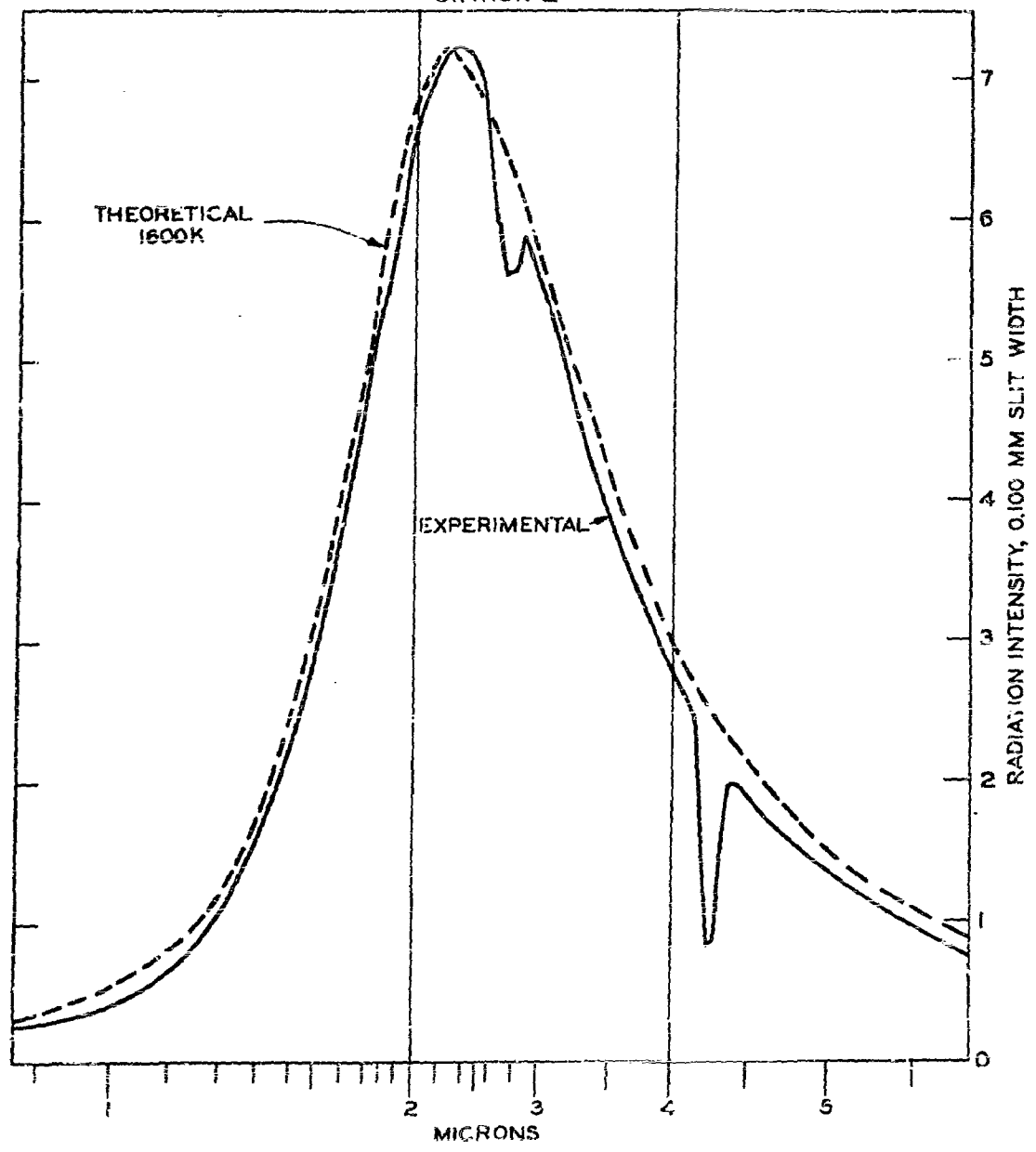
The emissivity of the flames seem to be somewhat less on the average in the 8 to 14 micron region than it is in the 2.5 micron region. This may be a function of the particle size of the incandescent material present in the flame, particularly in those luminous flames in which there is little or no exhaust smoke due to burning of the carbon formed in the flame zone.

B. Black-Body Considerations

In order to study the relationship between the continuous flame radiation in luminous flames and black body radiation the Globar emission was compared with a theoretical black body operating at the same temperature as the Globar. It was necessary to take into account the dispersion of the monochromator, the effective slit width of the monochromator and the emissivity of the Globar in order to make an approximate comparison. The dispersion data were obtained from the wavelength calibration of our monochromator. The emissivity of the Globar and the variation of effective slit width with wavelength were taken from information published by Bell (6). No account was taken of the variation in thermocouple blackness with wavelength of radiation striking it or linearity of thermocouple response.

Figure 24 is a comparison of the short wavelength experimental Globar radiation curve with a theoretical 1600 K Globar. The temperature of the Globar was measured by means of an optical pyrometer. The theoretical curve was obtained by calculating the 1600 K black body radiant energy distribution by Planck's equation $E_{\lambda} = C_1 \lambda^{-5} (e^{C_2/\lambda T} - 1)^{-1}$. E_{λ} is the radiant energy per unit area per unit increment of wavelength, λ , T is the absolute temperature, C_1 and C_2 are constants, and e is the Napierian base. This theoretical black body curve was then subjected to the dispersion curve of the monochromator by means of the relation $I_{\lambda}^0 = k E_{\lambda} \frac{d\lambda}{ds}$. I_{λ}^0 is the intensity of radiation as measured by the spectrophotometer, k is a normalizing factor and $\frac{d\lambda}{ds}$ is the dispersion at wavelength λ in terms of the monochromator wavelength drum scale readings, s . The curve thus obtained was further modified to take into account the emissivity of the Globar and the variation in effective slit width. Because of the variation in effective slit width the recorded intensity I_{λ} is related to I_{λ}^0 by relationship $I_{\lambda} = I_{\lambda}^0 (Se/S)^2$. Se and S are the effective and geometrical slit widths,

STATION 2



PHILLIPS PETROLEUM COMPANY
RESEARCH DIVISION REPORT 1176-56R

FIGURE 24

THEORETICAL AND EXPERIMENTAL GLOBAL EMISSION SPECTRA

respectively, which are related by $S_e = S - 1.7 \lambda$. The effect of variation of lens focal length with wavelength was not taken into account. The slit width used was the standard Figure 9 slit width, 0.100 millimeters. The normalization factor used will be discussed in connection with Figure 25. The agreement between the experimental and theoretical Globar curves is sufficiently close to warrant the comparison between the continuous flame emission and theoretical black body radiation curves.

Figure 25 shows the relationship between the station 5, condition 450, Figure 13, toluene flame emission and the theoretical black body radiation curves for 1800 K and 2000 K. Both of the black body curves have been normalized to the same peak intensity. In this case, the same corrections were applied to the black body curves as were applied for the theoretical curve in Figure 24 except that the geometrical slit width here is 0.07 millimeters. The normalization factors used for the 2200, 1800, and 1600 K (Figure 24) theoretical curves were in the ratio of 0.47, 1, and 0.38, respectively. The factor of nearly three between the 1800 and 1600 K curves is in large measure due to the losses of radiation encountered in the imaging of the Globar in the flame tube and inaccuracies in focusing the final infrared image at the slit of the monochromator.

Except for the spectral regions where the exhaust gas and atmospheric absorptions are evident the toluene flame emission curve agrees quite well with the 1800 K theoretical curve. This indicates that at wavelengths shorter than 6 microns the continuous radiation is indeed very nearly black body in character.

The deviation between the theoretical 1800 K and the station 5 toluene flame emission spectrum at wavelengths shorter than about one micron is probably due in part to smoke absorption. There appears to be little change in the intensities at wavelengths greater than one micron with large changes in exhaust smoke concentration although the visible radiation was almost completely obliterated in some cases at station 5 by the 28 inch column of smoke. Also under conditions of high emissivity the intensity of the radiation at stations 1 and 2, with no smoke between the flame and observer, is comparable with the station 5 intensity. This indicates that the smoke as such in the exhaust had little influence on the amount of infrared radiation from the toluene flame reaching an observer at station 5.

However, examination of the Figure 12, station 5, benzene spectra shows greater infrared radiation absorption by the smoke. In this case the condition 150 spectrum at wavelengths greater than 2.5 microns has about the same shape as the condition 450 spectrum, but the latter curve falls below the condition 150 curve at wavelengths less than 2.5 microns. This reduction in radiation intensity due to smoke increases as the wavelength decreases. The greater reduction in radiation intensity over a broader wavelength band in the case of benzene probably is associated with the amount and kind of smoke.

C. Flame Temperature

The shape of the dispersion function of the sodium chloride prism monochromator changes the shape of the familiar, linear in wavelength, black body energy distribution. The small dispersion in the two to four micron region peaks the radiation curve very sharply. If the linear in wavelength radiation intensity peak occurs at wavelengths less than three microns the prism dispersed intensity peak is at longer wavelengths. The displacement of the prism peak

PHILIPPS PETROLEUM COMPANY
RESEARCH DIVISION REPORT 1524-541

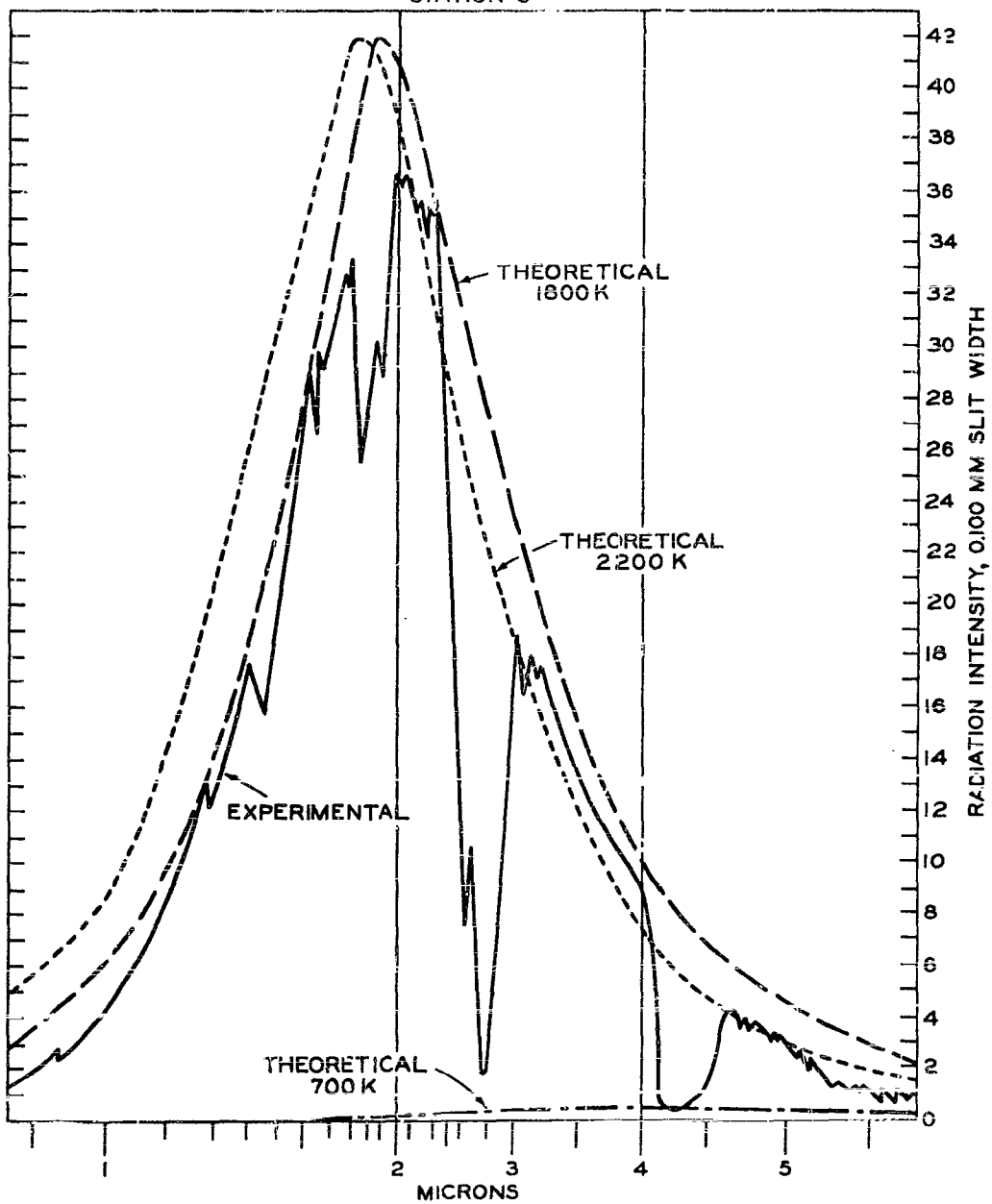


FIGURE 25
THEORETICAL BLACK BODY AND HIGH PRESSURE
TOLUENE FLAME EMISSION SPECTRA

toward longer wavelengths increases with decrease in the wavelength of the linear in wavelength intensity peak, i.e., at higher temperatures. At 1800 K the prism intensity peak shifts about 0.1 micron for a change in temperature of about 300 K. The shape and peak wavelength of the continuous radiation for the luminous flames, as well as the intensity in the four to five micron region for all flames at conditions 150 and 450, indicates that the temperatures are nearly the same for all the flames. Further, the luminous material in the flame appears to be at the same temperature as the carbon dioxide gas in the flame.

Inspection of the spectra indicates that the length of the primary combustion zone for the two aromatic fuels is less than for the two paraffinic fuels. This is shown primarily by the change of the station 3 radiation from luminous to non-luminous at condition 150. This, coupled with the higher emissivity of the two aromatic flames, and the consequent cooling by radiation loss may well account for the apparent constancy of temperature although the heat release for the two aromatic fuels is about 10 per cent less than for the two paraffinic fuels. In addition, benzene and toluene flames are cooler when compared to normal heptane and isooctane flames due to their increased carbon formation.

It has been pointed out (7, 8), that the intensity of the 4.4 micron carbon dioxide emission would be a good measure of the flame temperatures. In the case of the jet combustor it appears that the residence time within the primary combustion zone is sufficient to establish an apparent thermal equilibrium between the incandescent particles and the gas molecules. Within the primary combustion zone of the turbulent flames observed here probably in excess of 10^6 collisions occur per molecule. With a reasonable degree of interaction, on collision, between translation and vibrational excitation some degree of equilibrium between translational and vibrational temperatures may be expected.

Since the emissivity of the carbon dioxide radiation is essentially one for the two inch combustor at pressures above 150 inches of mercury and would approach one at lower pressures in larger scale combustors, the intensity of the carbon dioxide 4.4 micron radiation should serve as a good radiation thermometer. It would be unaffected by the luminosity of the flame and the temperature of the combustor walls seen through the flame. By making the measurement at a wavelength slightly longer than the atmospheric absorption band the measurement would be independent of the external optical path lengths. Since the emission band broadens toward longer wavelengths with increase in temperature and the intensity increases as a power greater than one with the temperature, the relative accuracy of such a pyrometer should increase with increased temperature. Since the incandescent particles appear to be in thermal equilibrium with the gas it would be reasonable to expect the carbon dioxide molecules to be nearly in thermal equilibrium with other gases in the flame.

Figure 26 shows the theoretical relationship between the intensity of the 4.4 micron emission (emissivity of one) and temperature. The intensity scale as well as the dispersion and slit width corrections are the same as those used in the 1800 K theoretical curve in Figure 25.

D. Total Radiation Measurement

The total radiant energy per unit area per unit time, E , emitted by a black body is the area under Planck's radiation intensity versus wavelength curve.

$$E = \int_{\lambda_1}^{\lambda_2} E_{\lambda} d\lambda$$

where λ_1 and λ_2 define the wavelength interval being considered.

PHILLIPS PETROLEUM COMPANY
RESEARCH DIVISION REPORT 1526-54R

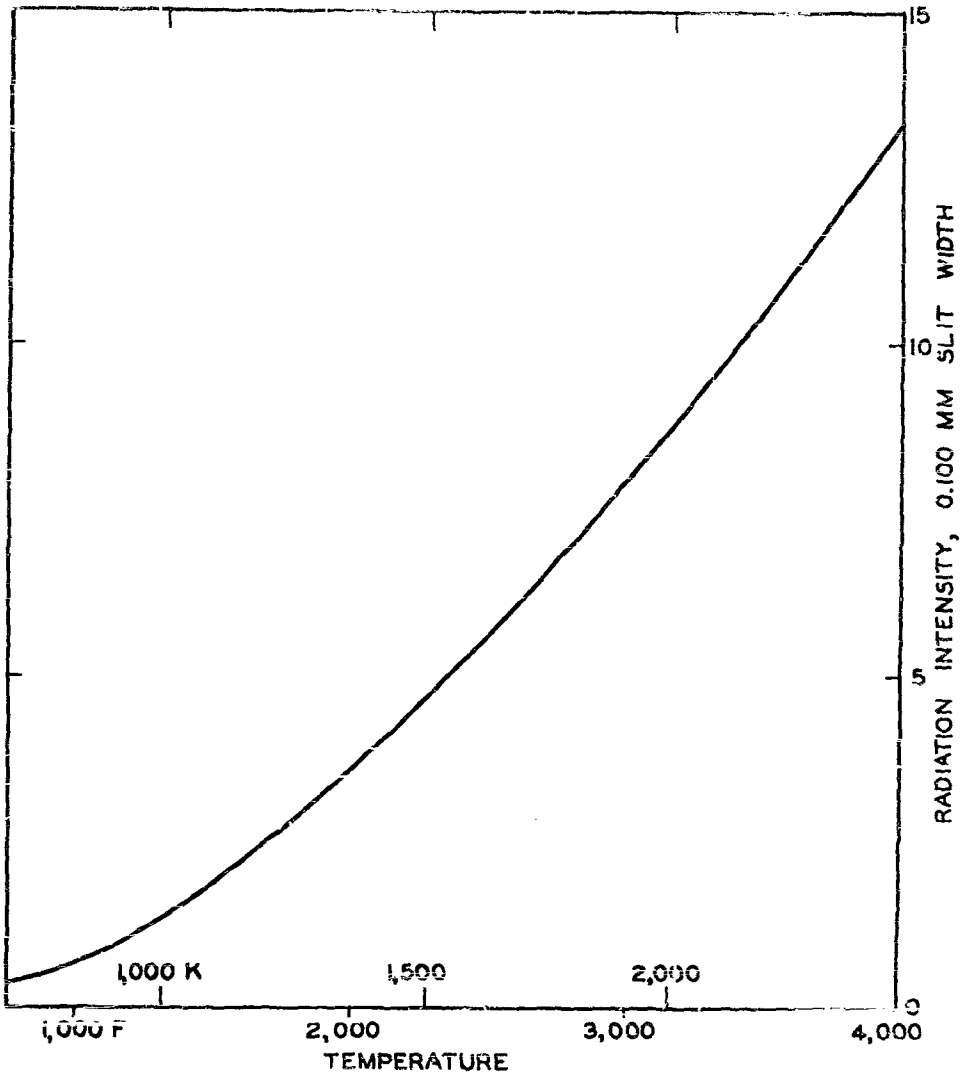


FIGURE 26
RADIATION INTENSITY AT 4.4 MICRONS VS TEMPERATURE

If I_λ is the radiation intensity at wavelength λ as seen by the spectrophotometer neglecting dispersion, effective slit width, etc.; then $I_\lambda = I_{\lambda'}^{\frac{d\lambda}{ds}}$ and $E = 1/k \int_{\lambda_1}^{\lambda_2} I_\lambda d\lambda$. The infrared spectrum is usually obtained at constant slit width but with a dispersion which is a function of wavelength. Therefore, the spectrophotometric spectrum of the black body will not look like the usual Planck's curve.

Taking dispersion into account but assuming a uniformly black receiver and a constant effective slit width, the intensity, I_λ , at wavelength λ will be recorded by the spectrophotometer as $I'_\lambda = I_\lambda \frac{d\lambda}{ds}$. $\frac{d\lambda}{ds}$ is the dispersion in terms of wavelength λ and the spectrometer drum scale, s . Rewriting in terms of the drum scale $I_s = I'_\lambda = I_\lambda \frac{d\lambda}{ds}$ describes the intensity which will be recorded by the spectrophotometer at drum reading s . Changing variables from λ to s by $d\lambda = \frac{d\lambda}{ds} ds$ and changing the limits of integration from λ_1 and λ_2 to the corresponding s_1 and s_2

$$E = 1/k \int_{s_1}^{s_2} I'_s \frac{ds}{d\lambda} \cdot \frac{d\lambda}{ds} ds = 1/k \int_{s_1}^{s_2} I'_s ds.$$

Thus except for second order corrections due to change in effective slit width as a function of wavelength [$S_e = f(\lambda)$] and variation in blackness of the detector with wavelength [Sensitivity = $f(\lambda)$] it is valid to integrate the spectrum as obtained from the spectrophotometer to obtain the total energy.

At a temperature of 1800 K about 90 per cent of the radiation emitted by a black body will be emitted at wavelengths shorter than five microns. This percentage drops to about 85 per cent at 1600 K and rises to more than 95 per cent at 2500 K. Therefore, in studying the total radiant energy from luminous flames the uncertainty induced by ignoring radiation of wavelengths greater than about five microns will not seriously prejudice our results. In the discussions that follow all energy integrations are over the range 0.87 to 5.8 microns. The uncertainty introduced in the case of the non-luminous flames is somewhat larger. The uncertainty of the trends deduced from the data is probably no larger than that due to lack of reproducibility of both flame conditions and instrument alignment.

Another source of error is the contribution of energy by the flame tube which is measured as flame radiation. In Figure 25 the 700 K curve shows the scale of the contribution to be expected from the flame tube if the area of the flame tube observed by the spectrophotometer is the same as the area of the flame observed. In the case of non-luminous flames this may become a sizable portion of the total radiation at wavelengths shorter than 5.8 microns.

Considering the non-luminous flame spectra in Figures 10 through 13 the continuous radiation present may be approximately synthesized from the 700 K and 1800 K curves of Figure 25. Making such a synthesis visually and transcribing the results in graphical form gives the data shown in Figure 27. This is a plot of the per cent of radiation in the 0.8 to 5.8 micron region due to molecular radiation of carbon dioxide and water together with the continuous radiation due to the flame tube walls (700 K) and the incandescent material in the flame (1800 K) versus observation station along the flame tube for the four fuels.

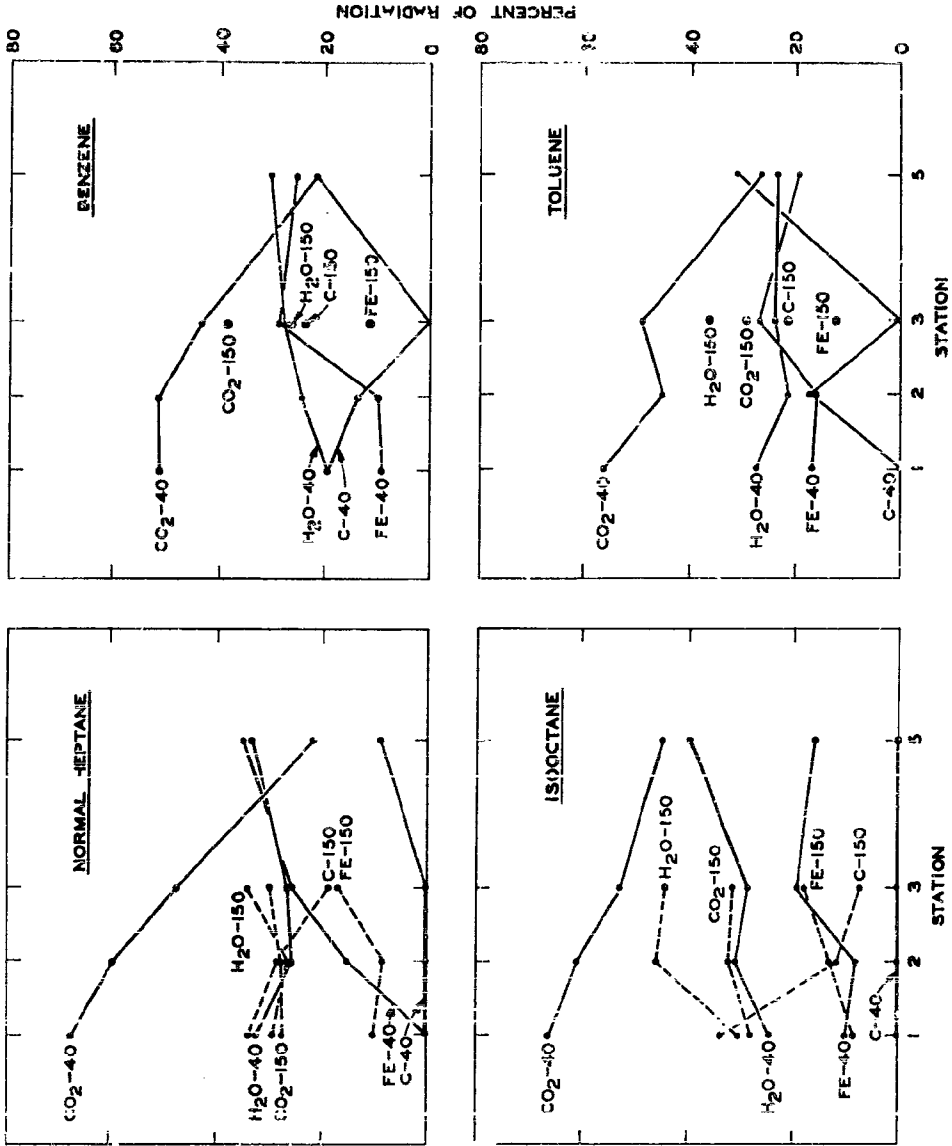


FIGURE 27
RADIANT ENERGY CONTRIBUTED BY VARIOUS SOURCES

The curves are labeled as to the sources of the radiation (CO_2 , H_2O , Fe, and C) and the combustor operating conditions (40 and 150). Fe and C represent the contributions due to the flame tube and the incandescent material, respectively.

The above flame tube contribution is included in the total radiant energy in the data shown in Figures 28 and 29. Further, no corrections are applied for effective slit width, receiver blackness, smoke, or atmospheric absorption.

From the Stefan-Boltzmann relationship, $E_T = \sigma T^4$, the total radiation, E_T , emitted by an 1800 K black body is 19.55 Btu per square foot per hour. The area under the 1800 K curve of Figure 25 was integrated and the resulting area set equal to the 19.55 Btu. Using this information the integrated area obtained from the experimental flame curves were then converted to Btu's per square foot per hour and plotted as such in Figures 28 and 29.

Figure 28 shows the variation of radiation intensity with position along the axis of the combustor for individual fuels at the three test pressures. The data are for observation stations 1, 2, 3, and 4.

Figure 29 shows the variation of radiation intensity with fuel type at test conditions 40, 150, and 450 for observation stations 1, 2, 3, and 5. Corroborating the earlier observations presented in Reference 1, it should be noted that the total radiation intensity at station 5 decreased for the two aromatic fuels when the combustor pressure was raised from 150 to 450 inches of mercury. This effect was most pronounced for benzene. This probably can be attributed to the smoke in the exhaust gases between the flame and station 5.

The information in Figure 30 is of a more speculative nature. We assumed that the density and character of the flame would not be changed in going to larger more practical sized combustors. The scaling factors used were 3X for diameter and 2X for length of the primary combustion zone. Figure 30 then shows for a hypothetical six-inch combustor the radiation intensity variation with fuel type at comparable operating conditions for various positions around the flame corresponding to stations 1, 2, 3, and 5 in the laboratory scale combustor. The station 5 situation indicates the radiation intensity to which a turbojet engine turbine nozzle might be exposed. These data were further simplified by assuming that the paraffinic fuels, normal heptane and isooctane, were nearly alike and that the two aromatic fuels, benzene and toluene, were nearly alike.

These extrapolations indicate that at low pressure and high velocity, test condition 40, there appears to be little significant variation with fuel type. At intermediate pressure with reduced velocity, test condition 150, there were significant differences in the radiant energy emitted by paraffinic and aromatic flames as seen from stations 1, 2, and 5 (nozzle). At high pressure with velocity the same, test condition 450, there appears to be less change in radiation intensity with fuel type. At station 3 the differences between the two fuel types were not large for any operating condition.

In making instrumental measurements of total radiant energy by means of a total radiation pyrometer using a black detector the transmission characteristics of a combustor window material are important. If the radiation is limited to wavelengths less than 2.5 microns by the use of Pyrex or Vycor window material, then the amount of radiation measured may give little indication of the amount of radiation present. The transmission spectrum of a typical Vycor combustor window is

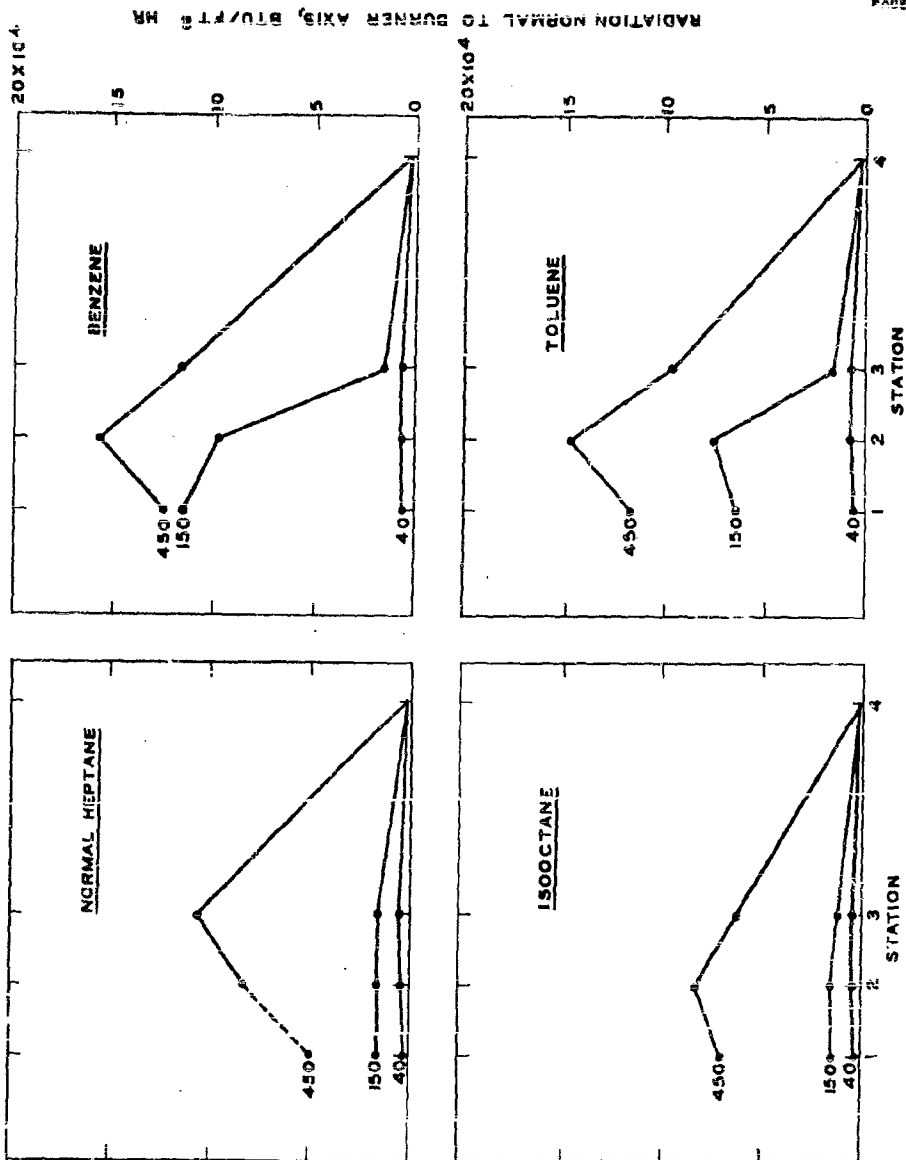


FIGURE 28
RADIATION INTENSITY VS POSITION ALONG COMBUSTION

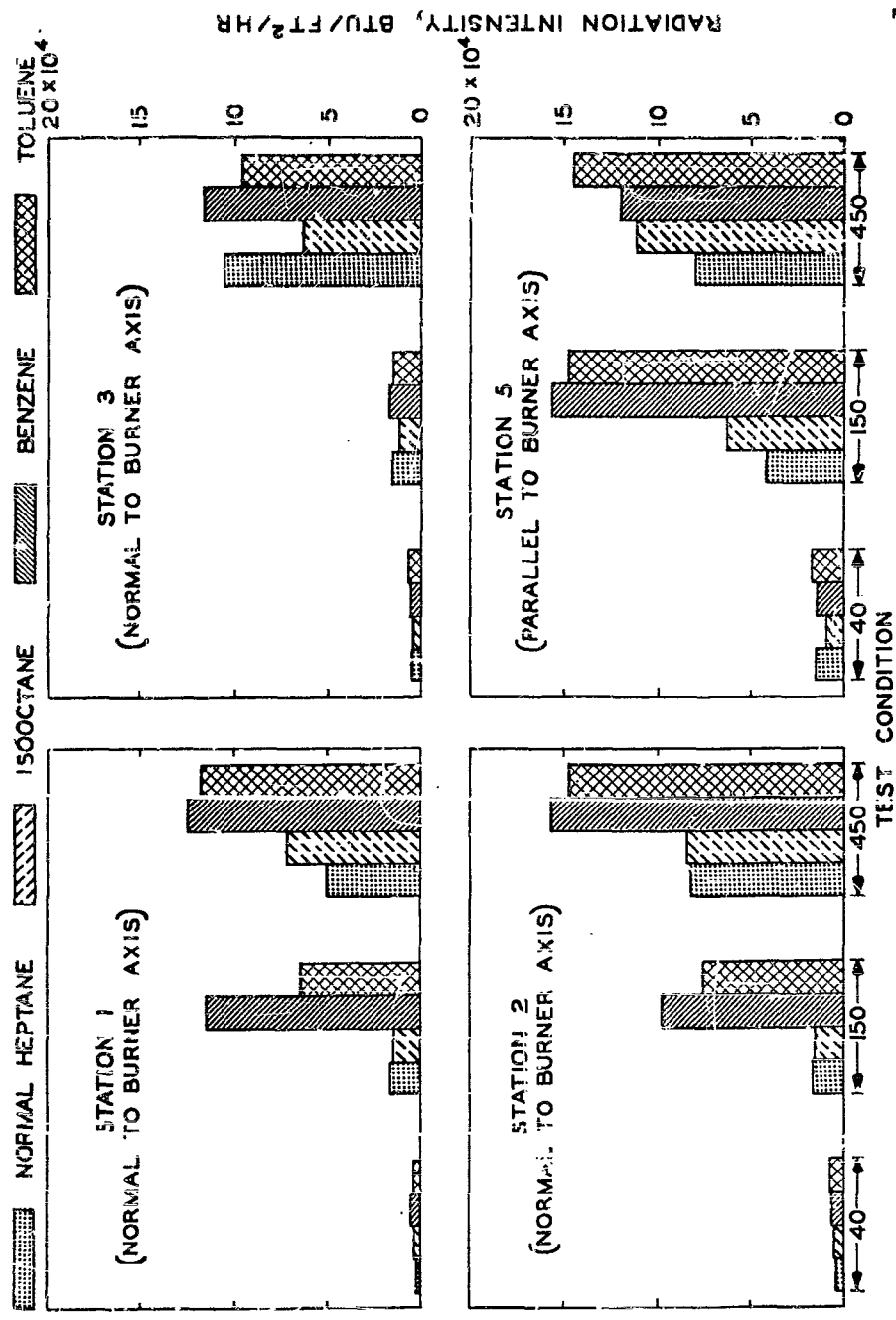


FIGURE 29
RADIATION INTENSITY VS OPERATING CONDITION

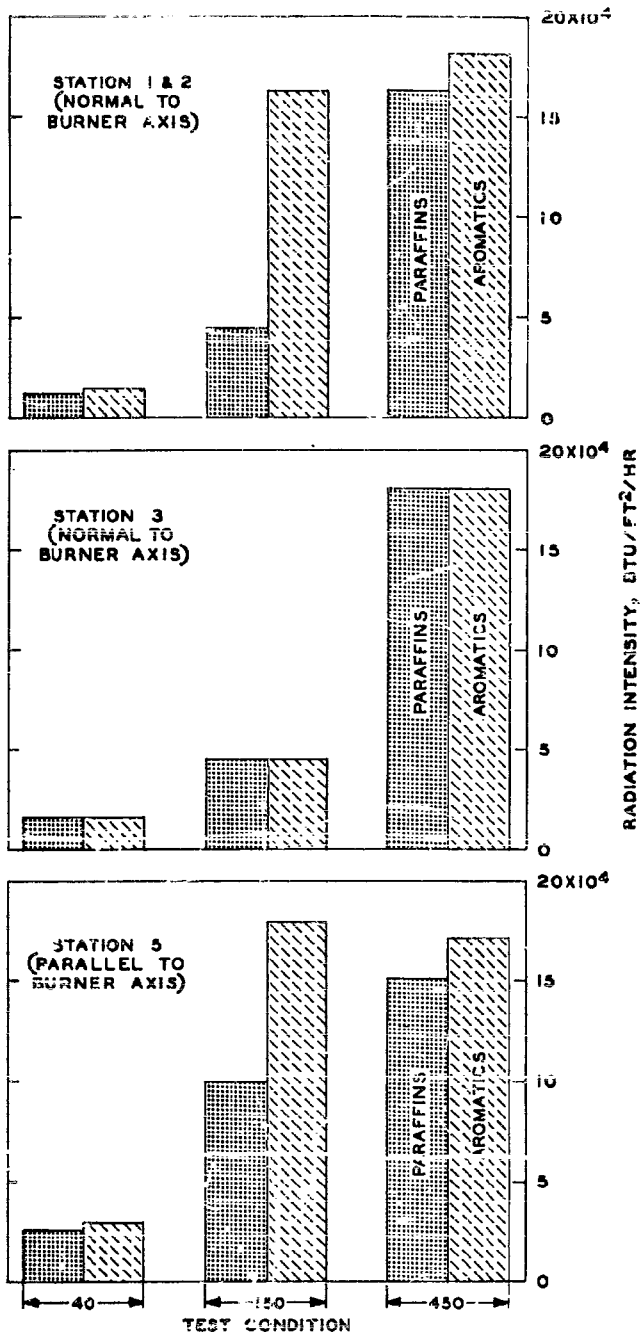


FIGURE 30
RADIATION INTENSITY FOR EXTENDED COMBUSTOR DIMENSIONS

shown in Figure 31. For 1800 K flame the ratio of the amount of radiation measured to the total will vary from a few per cent (about 2) to about 60 per cent depending upon the luminosity of the flame. The emissivity of the continuous radiation in a two-inch burner varies over wide limits from 0.01 to essentially one. In the non-luminous flame only a small percentage of the molecular radiation for small scale flames lies at wavelengths less than 2.5 microns.

As pointed out previously about 90 per cent of the continuous radiation from an 1800 K black body is at wavelengths shorter than 5.5 microns. Probably 75 per cent of the molecular radiation from the two-inch combustor has wavelengths shorter than this 5.5 microns. Thus, based on the combustor spectral data shown here, if observations of flame radiation are made through sapphire windows the data should give fairly reliable indications of the total amount of radiation present. However, if the observations are to be made through long columns of exhaust gases the absorption of the smoke must be taken into account. The transmission spectrum of typical sapphire and quartz combustor windows are shown in Figure 31.

There would be some advantage to extending the limiting wavelengths to ten microns by using calcium fluoride windows. This would include about 98 per cent of the 1800 K continuous radiation. A corresponding larger proportion of the molecular radiation would be included. However, the gain in the larger fraction of energy obtained would probably not offset the advantages of using the more rugged sapphire rather than the soft and somewhat fragile calcium fluoride.

E. Combustion Process

In the infrared absorption spectra of the experimental flames, Figure 19, the absorption due to carbon-hydrogen stretching vibration at 3.4 microns appears irregularly and is not strong compared to the raw fuel absorption in Figure 21. The 3.4 micron absorption is recognized only at test conditions 40 and 150. Further, it appears most frequently at stations 1 and 2. This suggests that upon entering the combustion zone the hydrogen is immediately stripped from the carbon chains by molecular collision or radiation absorption (vibrational excitation).

A comparison of the radiation spectra of the experimental flames and the absorption spectra of the fuels indicates that the radiative transfer of energy from the flame to the fuel is a somewhat inefficient process. This is particularly evident in non-luminous flames where the molecular radiation bands of the flame do not coincide with the absorption bands of the fuel. In the luminous situation the fuel absorbs over spectral regions containing about 10 per cent of the available energy. This is the result of the high intensity of the continuous radiation in the 3.4 micron region.

VI. SUPPLEMENTARY MEASUREMENTS OF COMBUSTION CLEANLINESS

Previous studies (Reference 1) have indicated a possible correlation between the intensity of flame radiation and

- (1) combustor metal temperature,
- (2) combustor metal loss rate,
- (3) combustor deposit formation rate, and
- (4) exhaust gas smoke density.

PHILLIPS PETROLEUM COMPANY
RESEARCH DIVISION REPORT 1524-548

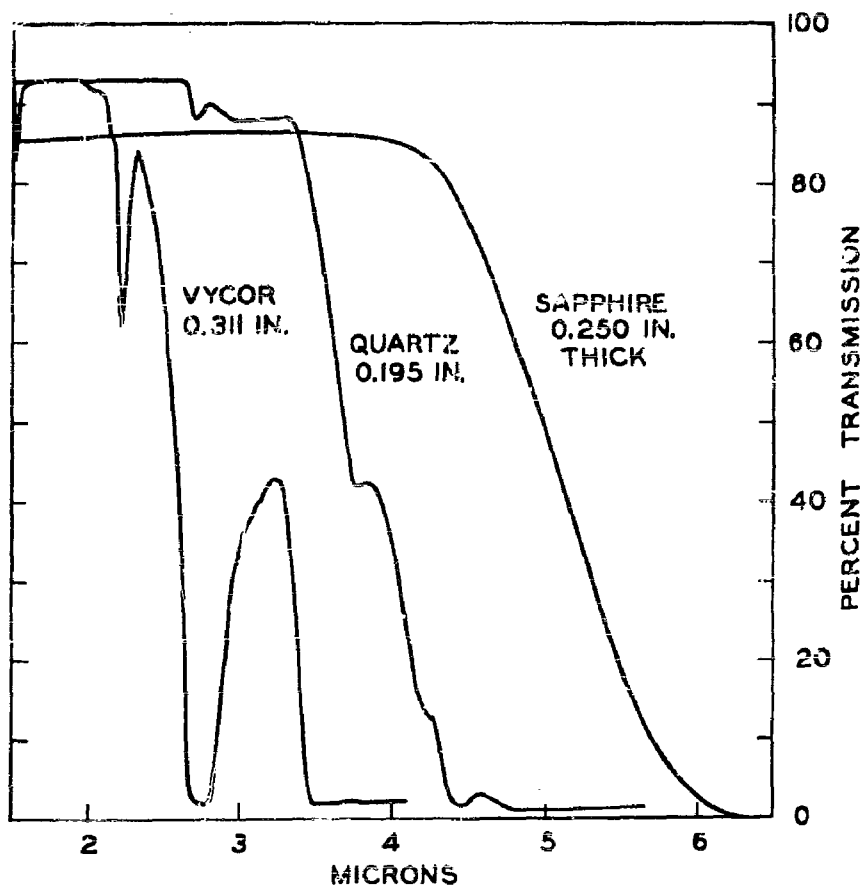


FIGURE 31
TRANSMISSION PROPERTIES OF WINDOW MATERIALS

These combustor performance variables are apparently interrelated by pyrolytic carbon formation, and therefore have been grouped under combustion cleanliness. To further investigate this premise supplementary measurements were made of these four parameters in conjunction with the principal flame radiation investigation, using the same four test fuels described in Table I and three test conditions detailed in Table II.

A. Combustor Metal Temperature

Combustor metal temperature has been measured in past studies by welding chromel-alumel thermocouples to the outer surface of the flame tube. Because of convective and conductive heat transfer this technique does not present a true picture of the flame tube inner surface temperature. It was also unsatisfactory because of the poor durability of the thermocouples and the difficulty in assembling such combustor test sections. Therefore, the flame tube and its related outer steel housing were modified for this test program. Ten adjustable immersion, closed-end, 1/16-inch diameter, Ceramo, chromel-alumel thermocouples were inserted through fittings in the combustor wall which were aligned with holes in the flame tube so that their temperature sensing tips fitted snugly and were flush with the flame tube inner surface. The locations of the thermocouples, which were in two rows on opposite sides along the axis of the combustor flame tube, are indicated in Figure 32. Subsequent testing has suggested that flame tube distortion, resulting in blow-by cooling of thermocouples, may have produced indicated temperature too low by several hundred degrees F.

The detailed flame tube inner surface temperature data obtained are presented in Table III. To more clearly show the effect of the three combustor operating conditions, the averaged data are plotted separately for each of the four test fuels in Figure 33. These plots allow interpolation of flame tube inner surface temperature at the locations surveyed for flame radiation. The combustor metal temperature data thus obtained are plotted in Figure 34 to facilitate comparison with Figure 29.

Comparison of the combustor metal temperature data in Figure 34 with the total flame radiant energy data in Figure 29 shows that a general correlation does exist between these two variables.

The data illustrate quite clearly that increases in flame tube inner surface temperature usually accompany increased combustor operating pressure.

While the hydrocarbon structure of the test fuels showed little influence upon flame tube inner surface temperature at the lowest combustor operating pressure, the primary combustion zone ran up to several hundred degrees hotter with the two aromatic fuels at the intermediate pressure operating condition, 150. This correlates with the higher emissivity and shorter flame lengths shown in Figure 28 at the intermediate pressure with these aromatic fuels. It is interesting to note that at the highest pressure operating condition, 450, these differences in combustor metal temperature diminish again. This probably is the result, at some locations as shown in Figure 33, of a decrease in metal temperature with the two aromatic fuels. A comparable decrease in radiation intensity was also observed with the two aromatic test fuels at station 5 in Figure 29, which is in agreement with the preliminary observations presented in Reference 1. In the latter case, where operating conditions were even more conducive to pyrolytic carbon formation, the decrease in radiation intensity obtained with the aromatic test fuel, benzene, was of sufficient magnitude to result in an actual reversal, with the paraffinic test fuels, normal heptane and isooctane, producing higher radiation intensities.

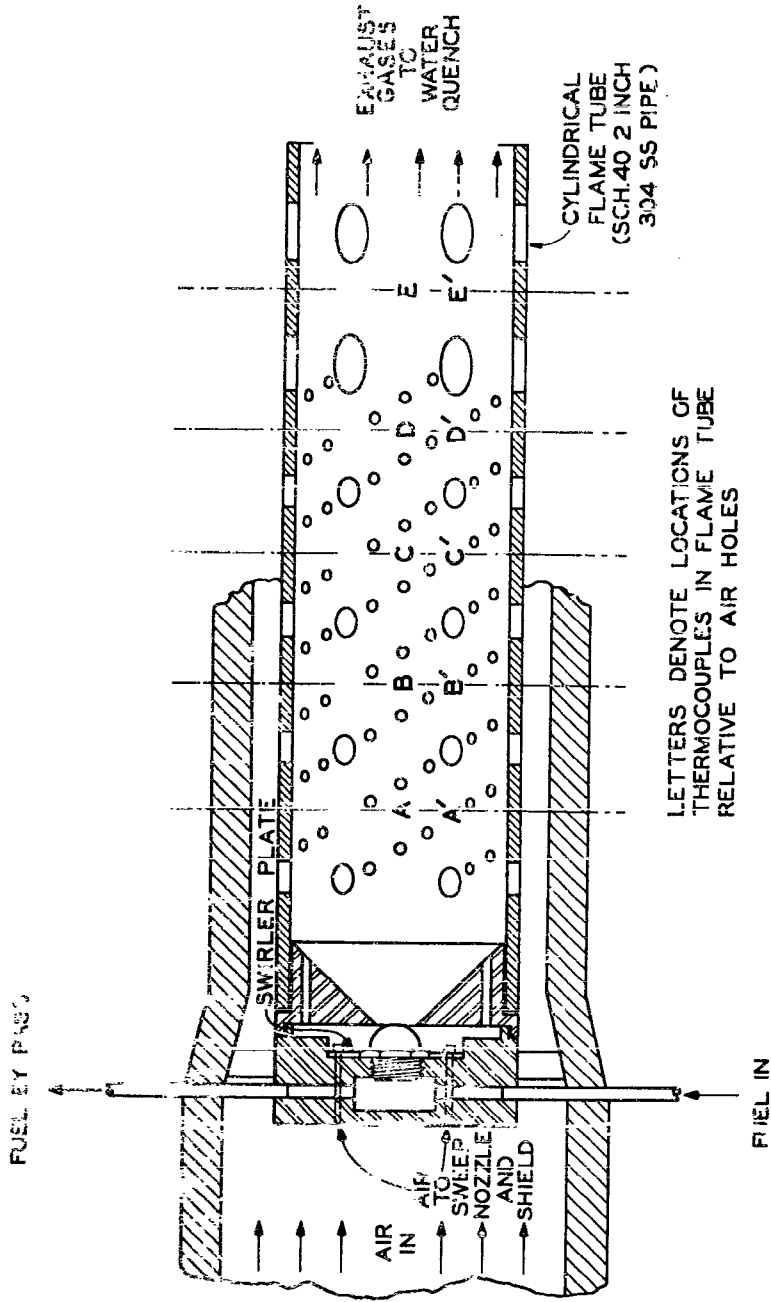


FIGURE 32
DIAGRAM OF COMBUSTOR SHOWING THERMOCOUPLE LOCATIONS

UNCLASSIFIED

**A
D
138244**

Armed Services Technical Information Agency

Reproduced by

DOCUMENT SERVICE CENTER

KNOTT BUILDING, DAYTON, 2, OHIO

FOR
MICRO-CARD
CONTROL ONLY

2 OF 2

NOTICE: WHEN GOVERNMENT OR OTHER DRAWINGS, SPECIFICATIONS OR OTHER DATA ARE USED FOR ANY PURPOSE OTHER THAN IN CONNECTION WITH A DEFINITELY RELATED GOVERNMENT PROCUREMENT OPERATION, THE U. S. GOVERNMENT THEREBY INCURS NO RESPONSIBILITY, NOR ANY OBLIGATION WHATSOEVER; AND THE FACT THAT THE GOVERNMENT MAY HAVE FORMULATED, FURNISHED, OR IN ANY WAY SUPPLIED THE SAID DRAWINGS, SPECIFICATIONS, OR OTHER DATA IS NOT TO BE REGARDED BY IMPLICATION OR OTHERWISE AS IN ANY MANNER LICENSING THE HOLDER OR ANY OTHER PERSON OR CORPORATION, OR CONVEYING ANY RIGHTS OR PERMISSION TO MANUFACTURE, USE OR SELL ANY PATENTED INVENTION THAT MAY IN ANY WAY BE RELATED THERETO.

UNCLASSIFIED

TABLE III
EFFECT OF TUBE TYPE AND OPERATING CONDITIONS ON CONDENSOR PLATE TUBE TEMPERATURES

Test Condition (See Table II) Thermocouple Location (See Fig. 32) Fuel (See Table I)	Plate Tube Inner Wall Temperature, F.															
	40				150				450							
	A/A'	B/B'	C/C'	D/D'	E/E'	A/A'	B/B'	C/C'	D/D'	E/E'	A/A'	B/B'	C/C'	D/D'	E/E'	
Normal Heptane	430	450	800	760	800	840	850	880	710	870	1040	1060	1120	1040	870	
	470	720	740	900	810	680	732	810	870	800	710	680	770	1070	1090	
	490	590	770	830	805	760	835	830	840	885	885	870	845	1075	985	
	440	460	380	400	770	570	370	460	540	970	910	860	1020	780	670	560
	680	710	580	240	820	780	790	740	1160	1092	640	860	780	1210	780	1210
Toluene	580	585	480	670	795	675	575	800	820	1010	715	895	895	785	1085	
	505	587	525	740	800	717	745	755	830	947	850	882	922	890	1072	
	390	400	620	790	730	800	800	960	710	810	1010	1070	890	830	870	
	420	410	615	785	765	750	755	825	855	810	825	800	880	820	1120	
	405	520	615	785	765	750	755	825	855	810	825	800	880	820	1120	
Benzene	590	390	560	400	710	600	590	520	510	940	800	890	910	660	850	
	480	610	680	710	690	780	740	800	1090	1130	540	640	740	780	1060	
	587	500	620	655	715	675	685	680	810	1035	670	745	825	790	950	
	445	510	578	722	770	712	715	752	835	922	747	772	805	830	995	
	500	500	840	620	700	1220	1240	1290	865	890	1090	1050	1220	890	820	
Toluene	460	670	610	520	722	990	1008	810	840	810	720	650	700	880	1100	
	430	285	725	710	715	1100	1060	1060	915	670	905	850	880	885	965	
	530	520	540	400	740	710	660	660	480	820	530	1000	1110	640	940	
	640	590	660	890	810	1340	1160	1140	880	880	680	980	1040	820	1010	
	565	555	600	645	715	1085	950	735	810	895	580	990	1075	730	1010	
Toluene	552	570	662	677	742	1072	1010	897	862	868	992	920	1017	807	910	
	370	380	590	510	600	1270	1240	1310	950	890	930	900	1100	300	910	
	520	520	710	720	580	700	710	1010	940	870	920	820	960	280	1110	
	435	480	550	615	595	1045	975	1010	945	870	930	860	1090	890	1110	
	570	560	540	070	840	860	650	850	610	900	820	810	940	610	1140	
Toluene	890	820	800	1000	730	1070	870	890	1090	1010	770	1060	1120	870	1110	
	700	660	670	785	785	905	860	890	890	985	795	935	1035	790	1115	
	565	580	610	690	695	1005	917	930	898	927	852	898	1032	840	1152	
	565	580	610	690	695	1005	917	930	898	927	852	898	1032	840	1152	
	565	580	610	690	695	1005	917	930	898	927	852	898	1032	840	1152	

PHILLIPS PETROLEUM COMPANY
RESEARCH DIVISION REPORT 1524-54R

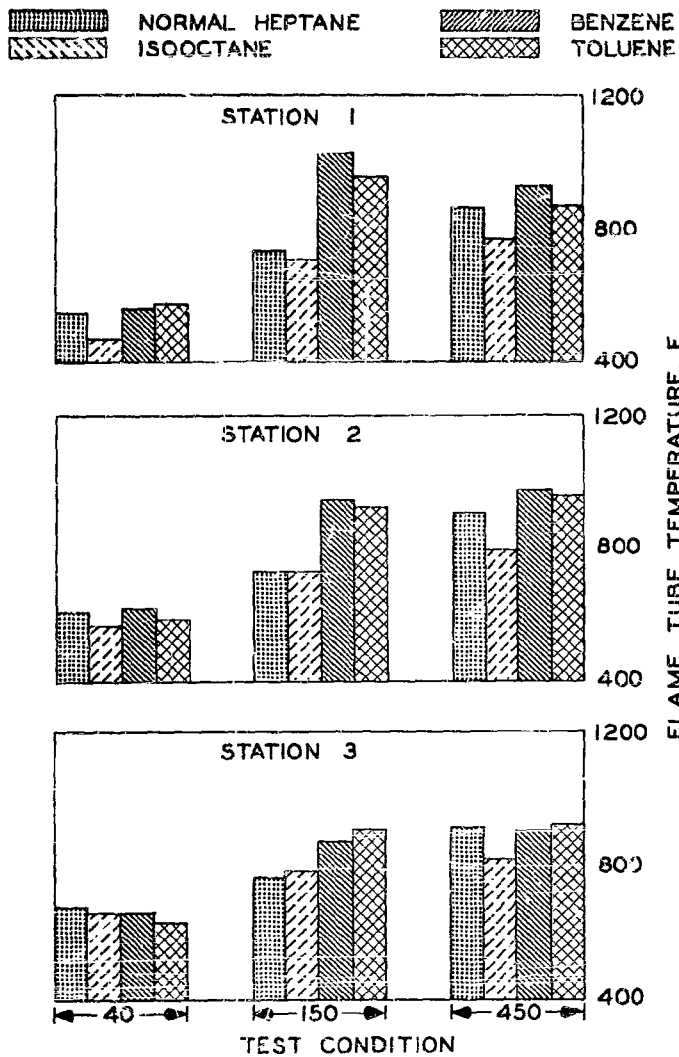


FIGURE 34
FLAME TUBE TEMPERATURE VS OPERATING CONDITION

Methods for reducing the higher primary combustion zone wall temperature obtained with similar aromatic fuels are suggested by the apparent independence of the flame tube inner surface temperature with respect to fuel type following the first major injection of secondary quench air, as indicated by the thermocouples E-E'. Unification of combustor design to increase the channels for conductive heat transfer and organization of flow patterns for control of convective heat transfer are indicated; however, simple insulation of the primary combustion zone wall by radiation shielding would be of considerable benefit.

B. Combustor Metal Loss Rate

A measurement of combustor durability was obtained from the difference in cleaned flame tube weight before and after testing. The Type 304 stainless steel flame tubes were thoroughly cleaned of all deposits and scale by wire brushing. Rates of metal loss were established by running one hour endurance type tests.

Table IV presents the data obtained on combustor metal loss rate, as well as that on combustor deposit formation rate and exhaust gas smoke density, because these three supplementary measurements were all made concurrently. No attempt was made to obtain data at the low pressure test condition, 40, because previous studies have shown negligible metal loss, deposits and smoke at such combustor operating conditions. The flame tube metal loss data obtained at the two higher pressures, while maintaining other operating variables constant, are plotted for all four test fuels in Figure 35.

These data show that increasing the combustor pressure increased the flame tube metal loss rate. This is compatible with the observed increase in radiant energy from the flame and higher flame tube inner surface temperatures previously noted. These data confirm previous indications of intensification of combustor durability problems at high pressure and temperature conditions for combustion.

The effect of the hydrocarbon structure of the test fuels on combustor metal loss rates are as would be expected from the differences observed in total flame radiant energy. Specifically, the paraffins, isooctane and normal heptane, produced lower rates of flame tube metal loss than the aromatics, toluene and benzene. Recent work (9) has shown that relief from this thermal erosion can be obtained by the choice of more resistant alloys, in addition to the above indicated selection of fuel hydrocarbon type.

C. Combustor Deposit Formation Rate

A measurement of the rate of formation of combustor deposits was obtained from the difference in flame tube weight before and after cleaning. The Type 304 stainless steel flame tubes were weighed following one hour endurance type tests, and then thoroughly cleaned of all deposits and scale by wire brushing for reweighing. The substantial variations in fuel flow rate, shown in Table II for the different operating conditions, were compensated for by presenting the data on a fuel weight ratio basis; that is, in terms of the weight of deposit formed per unit weight of fuel burned.

TABLE IV

EFFECT OF FUEL TYPE AND OPERATING PRESSURE ON METAL LOSS, DEPOSITS AND SMOKE

<u>Test Fuels</u>	<u>Test Conditions</u>	<u>Combustor Deposit Formation Rate</u>		<u>Combustor Metal Loss Rate</u>	<u>Exhaust Gas Smoke Density Percent Black</u>
<u>(See Table I)</u>	<u>(See Table II)</u>	<u>mg/hr</u>	<u>mg/kg Fuel</u>	<u>mg/hr</u>	
Normal Heptane	150	270	6.8	320	1
	450	920	8.6	2240	7
Isooctane	150	95	2.4	115	2
	450	790	7.4	990	21
	450	1100	10.2	1140	13
Benzene	150	1330	33.5	2190	23
	150	960	24.2	3110	-
	450	1500	14.0	4150	60
Toluene	150	4360	122.5	1190	15
	450	1090	10.2	2850	55

PHILLIPS PETROLEUM COMPANY
RESEARCH DIVISION REPORT 1238-56R

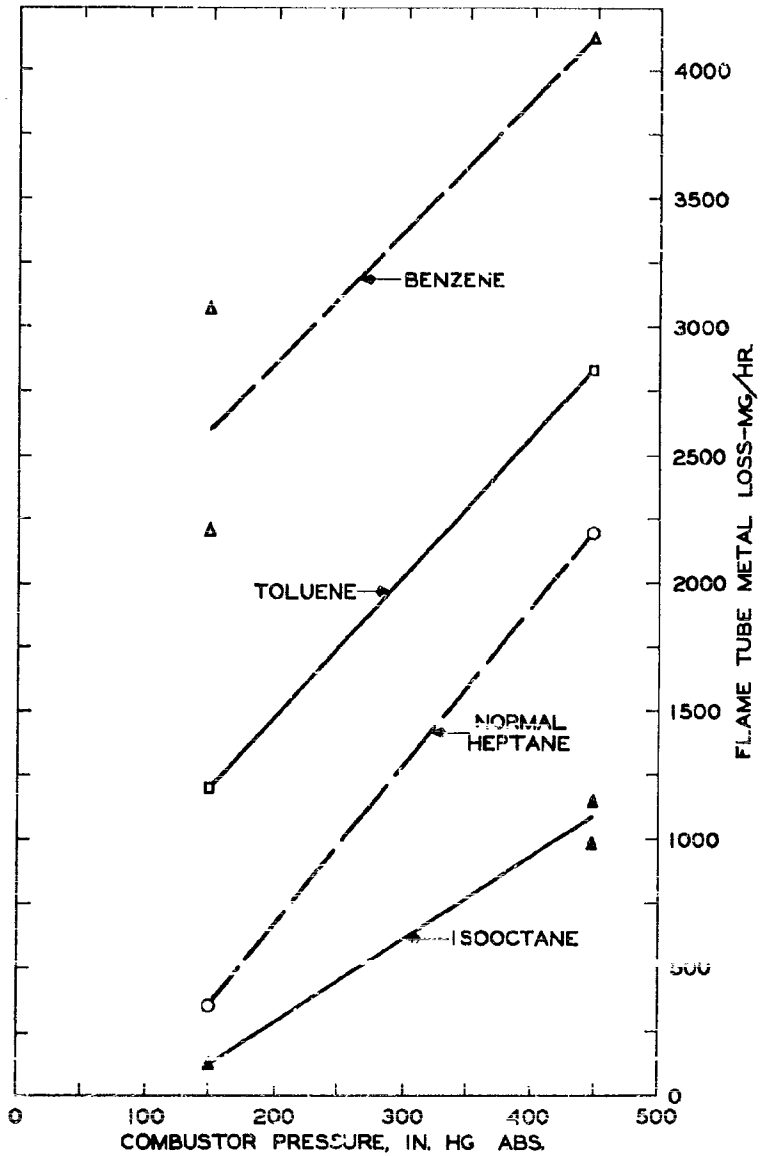


FIGURE 35
FLAME TUBE METAL LOSS VS COMBUSTOR PRESSURE

As pointed out in the preceding section on combustor metal loss rate, the concurrently measured data on combustor deposit formation rate are presented in Table IV. The flame tube deposit formation rate data obtained at the two higher pressures are plotted for all four test fuels in Figure 36.

Previous studies of combustor deposits (1) have indicated that deposition rate generally peaks at a moderate combustor operating pressure, falling between 100 and 200 inches of mercury. The present data appear to verify such an optimum pressure for combustor deposit formation rate. The reduction in carbonaceous deposits as combustor operating pressure exceeds five atmospheres has been attributed to their ignition and burn-off from the hot flame tube metal surfaces, rather than from lessened pyrolytic carbon formation. This is compatible with the greater flame radiant energy, increased flame tube inner surface temperature, and increased metal loss rates already discussed.

The effect of the hydrocarbon structure of the test fuels on combustor deposit formation rate were as would be expected, when deposits were obtained; that is, less deposits were produced by the paraffins, isooctane and normal heptane, than the aromatics, toluene and benzene. However, the most important observation was the continued indication that regardless of fuel hydrocarbon structure the combustor problems directly connected with carbon deposition were associated with only a limited combustor operating regime. This suggests that restrictions on fuel hydrocarbon type, which are dictated by combustor carbon deposition problems, simply reflect temporary combustor design and/or metallurgical limitations.

D. Exhaust Gas Smoke Density

A measurement of the amount of pyrolytic carbon in the combustor exhaust was obtained by filtering a constant stream of this gas through a strip of paper. This was accomplished by employing the E. K. Von Brand continuously recording gas sampler, connected through a sampling chamber to a 1/16-inch diameter total pressure type sampling probe. The sampling chamber was vented to the atmosphere. The smoke traces on the filter paper were assigned reflectometer readings with the aid of a Welch Densichron, which are a percentage of the blackness of a standard reference plate compared to a clean white filter paper.

As pointed out in the preceding section on combustor metal loss rate, the concurrently measured data on exhaust gas smoke density are presented in Table IV. The exhaust gas smoke density data obtained at the two higher pressures are plotted for all four test fuels in Figure 37.

The data illustrate quite clearly that increases in exhaust gas smoke density accompanied increased combustor operating pressure. This is in agreement with previous studies (1) which have indicated that increasing pressure probably promotes the formation of pyrolytic carbon by decreasing the rate of diffusion and mixing of the fuel and air. A relationship between the intensity of radiant energy from a flame and the concentration of black body radiators, of which smoke density is an index, is indicated. The difference in the two aromatic, 1 to 2.5 micron, station 5 spectra (Figure 12 and 13) indicate that there may be a difference in the benzene and toluene smoke other than the amount present.

While the density of exhaust smoke has not as yet been considered an operational limitation, its control may be desired for other reasons. Compensation for the decreased rate of micro-mixing accompanying increased charge density

PHILIPS PETROLEUM COMPANY
RESEARCH DIVISION REPORT 1128-SM

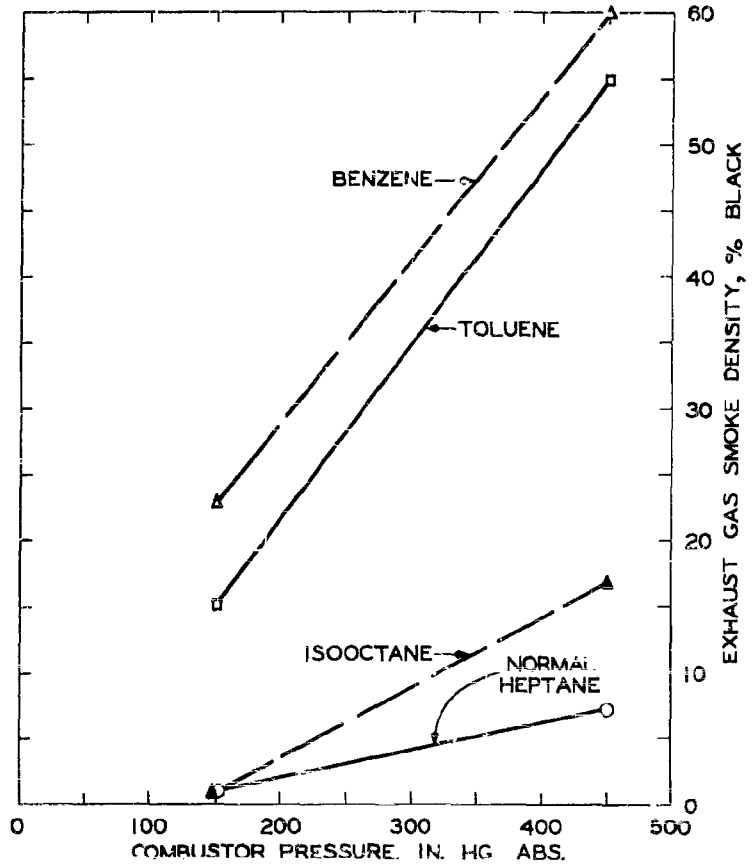


FIGURE 31
EXHAUST GAS SMOKE DENSITY VS COMBUSTOR PRESSURE

can be sought in more effective combustor design for micro-mixing of the fuel and air. Pre-vaporization of the fuel, to counteract the effective loss in velocity with increased pressure, represents one design approach through fuel preparation to more effective mixing.

It has long been recognized that the various hydrocarbon type fuels differ in their tendency to smoke. The effect of hydrocarbon structure on exhaust gas smoke density is as expected for the data obtained, with less smoke produced by the paraffins, isooctane and normal heptane, than the aromatics, benzene and toluene. However, under the severe combustor operating conditions which favor the formation of substantial quantities of pyrolytic carbon, little relief can be expected from restrictions on fuel hydrocarbon type.

VII. CONCLUSIONS

The following are short restatements of what are believed to be the significant findings of this work. They are relative to the laboratory scale jet combustor used, under the particular experimental conditions of this study.

(1) Non-luminous flames were characterized by discontinuous radiation, i.e., band emission of molecular origin. The emissivity in these molecular bands approached one only in the carbon dioxide, 4 to 5 micron, band. The average transverse emissivity, of the infrared spectral region from 1 to 15 microns in wavelength, was approximately 0.03.

(2) Luminous flames were characterized by a predominance of continuous radiation, which was black body in nature. For intermediate values of luminosity the discontinuous molecular radiation was evident, superimposed on the continuous black body radiation. The transverse emissivity of the continuous radiation varied from a few hundredths to nearly one, depending upon experimental conditions.

(3) In general, the emissivity of both the non-luminous and luminous flames increased with combustor pressure.

(4) The emissivity of the flames varied with fuel type when burned under constant combustor operating conditions. In general, the emissivities of the two aromatic fuels, benzene and toluene, appeared to be higher than that of the two paraffinic fuels, normal heptane and isooctane. This difference decreased at the highest combustor operating pressure, 450 in. Hg abs.

(5) In luminous flames, the heat transferred by radiation to combustor flame tubes, etc., was an appreciable portion of the total energy released. The radiative power varied from less than one per cent to greater than ten per cent of the total energy released, depending upon fuel type and operating conditions.

(6) Combustor flame tube metal temperatures increased with increasing combustor pressure (with decreasing combustor inlet velocity) and the associated increased flame emissivity.

(7) The effects of fuel type on flame tube metal temperature were negligible at the low pressure (30 in. Hg abs.) high velocity (350 fps) condition. At the two higher pressures (150 and 450 in. Hg abs.) and lower velocity (200 fps), the two aromatic fuels produced higher metal temperatures, agreeing with total radiation trends.

(8) Flame tube metal burn-off rates, at the two higher pressures, increased with metal temperature. Metal losses increased with pressure, and highest for benzene.

(9) Smoke, as such, had little to do with the radiative energy transfer through short columns, i.e., the absorption of infrared radiation by smoke was small. However, smoke forming tendency is important in that it governs the luminosity of the flame, and thus the radiative characteristics of the flame.

(10) Exhaust gas smoke density increased with pressure, and was highest for the two aromatic fuels. This indicates a direct relationship between pyrolytic carbon formation and radiant energy transfer in high pressure jet combustor flames.

(11) Flame tube deposit formation rates were highest at the intermediate pressure (150 in. Hg abs), with toluene producing the most deposits. At the highest pressure (450 in. Hg abs) deposits were low with all fuels tested.

(12) Flame "noisiness" (fluctuations of radiation intensity and transmission properties) was a direct function of the carbon forming tendency of the flame.

(13) The temperature of the flames studied here (fuel-air ratio 0.01) remained essentially constant over a large range of combustor operating conditions and fuel types. The temperature was in the neighborhood of 1800 K (2800 F) for the particular conditions of this study.

(14) The emissivity of the carbon dioxide 4 to 5 micron molecular emission was nearly one over a large range of operating conditions and fuel types. This indicates that the intensity of radiation in this spectral region is a good indication of the flame temperature and is essentially independent of the luminosity of the flame.

(15) The temperatures of the luminous material in the flame and the carbon dioxide gas appear to be very nearly the same.

(16) Narrow band-pass pyrometers adjusted for, say, the 4.4 micron region should serve as good flame thermometers if the flame cross section is sufficiently large (i.e., at least two inches thick).

(17) The molecular emission and absorption bands will broaden toward long wavelengths with increase in gas temperatures, making narrow band-pass pyrometry independent of atmospheric absorption. In addition, as a consequence of more material being present, the intensity of emission (i.e., emissivity) and absorption will increase with pressure at these longer wavelengths.

(18) Total radiation pyrometers must include the 1 to 5 micron spectral region to give reliable indications of the total infrared radiation emitted by the flame. Window material for such pyrometry is important. Sapphire windows will give substantially more reliable results than quartz without large luminosity and smoke corrections.

(19) Little hydrocarbon as such was present in the flame zone.

(20) Radiative energy transfer from the flame zone to the hydrocarbon fuel was relatively inefficient due to the non-coincidence of the absorption spectra of the fuel and the emission spectra of the flame. This was more pronounced in the case of non-luminous flames than in luminous flames.

VIII. REFERENCES

- (1) Kittredge, G. D.; Summary Report - Navy Contract N0as 52-132-c, Amendments 7-12. "Evaluation of Fuel Characteristics in Thermojet Engine Combustion Processes". Phillips Research Division Report 1237-55R, September, 1955. CONFIDENTIAL.
- (2) Topper, Leonard; "Radiant Heat Transfer From Flames in a Single Tubular Turbojet Combustor". NACA Research Memorandum RM 152F23, August 19, 1952.
- (3) Winter, E. F.; "Heat Transfer Conditions at the Flame Tube Walls of an Aero Gas Turbine Combustion Chamber". Fuel, Vol. 24, October 1955, pp. 409-428.
- (4) Berlad, A. L. and Hibbard, R. R., "Effect of Radiant Energy on Vaporization and Combustion of Liquid Fuels". NACA Research Memorandum RM 52109.
- (5) Fromm, E. H.; "Design and Calibration of Phillips Jet Fuel Testing Facilities". Phillips Research Division Report 1252-52R, December, 1955.
- (6) Bell, Ely E., Burnside, Phillips B., Cerman, Warren C., Dam, Cecil F., and Ryan, John F.; Study of Infrared Emission from Flames. Ohio State University--Research Foundation, Air Force Contract AF 30(602)-1047, Final Report--Part I, June 1955.
- (7) Gaydon, A. G. and Wolfhard, H. G.; Flames--Their Structure, Radiation and Temperature. Chapman and Hall, 1953.
- (8) Lewis, Bernard and Elbe, C. von; Combustion, Flames and Explosions of Gases. Academic Press, 1951.
- (9) Kittredge, G. D., Gwinn, S. H., and Streets, W. L., "Gas Turbine and Jet Engine Fuels. Navy Contract N0as 52-132-c, Amendment 13. Progress Report No. 6." Phillips Research Division Report 1525-56R, August 1956.
- (10) Parsons, J. L., Irland, M. J., and Bryan, F. H., "Continuous Flow Infrared Gas Analyzer Employing Interference Filters", Jour. Opt. Soc. Am., Vol. 46, p. 164 (1956).

UNCLASSIFIED

UNCLASSIFIED